Available online at www.sciencedirect.com
ScienceDirect
ELSEVIER
Biochemical and Biophysical Research Communications 351 (2006) 1078–1082
BBRC
www.elsevier.com/locate/ybbrc

Increased hypothalamic 5-HT2A receptor gene expression and effects of pharmacologic 5-HT2A receptor inactivation in obese A^y mice

Katsunori Nonogaki *, Kana Nozue, Yoshitomo Oka

Center of Excellence, Division of Molecular Metabolism and Diabetes, Tohoku University Graduate School of Medicine, 2-1 Seiryo-machi, Aoba-ku, Sendai 980-8575, Japan

Received 29 October 2006
Available online 7 November 2006

Abstract

Serotonin (5-hydroxytryptamine; 5-HT) 2A receptors contribute to the effects of 5-HT on platelet aggregation and vascular smooth muscle cell proliferation, and are reportedly involved in decreases in plasma levels of adiponectin, an adipokine, in diabetic subjects. Here, we report that systemic administration of sarpogrelate, a 5-HT2A receptor antagonist, suppressed appetite and increased hypothalamic pro-opiomelanocortin and cocaine- and amphetamine-regulated transcript, corticotropin releasing hormone, 5-HT2C, and 5-HT1B receptor gene expression. A^y mice, which have ectopic expression of the agouti protein, significantly increased hypothalamic 5-HT2A receptor gene expression in association with obesity compared with wild-type mice matched for age. Systemic administration of sarpogrelate suppressed overfeeding, body weight gain, and hyperglycemia in obese A^y mice, whereas it did not increase plasma adiponectin levels. These results suggest that obesity increases hypothalamic 5-HT2A receptor gene expression, and pharmacologic inactivation of 5-HT2A receptors inhibits overfeeding and obesity in A^y mice, but did not increase plasma adiponectin levels.

Keywords: 5-HT2A receptor; Sarpogrelate; 5-HT2C receptor; A^y mice; Pro-opiomelanocortin; Cocaine- and amphetamine-regulated transcript; Corticotropin releasing hormone; Obesity; Adiponectin; Hyperglycemia

A^y mice have dominant alleles at the agouti locus (*A*), which produces ectopic expression of the agouti peptide, an antagonist of the hypothalamic MC4 receptors and MC3 receptors [1–3], and display hyperphagia and obesity. A^y mice are reportedly resistant to the anorexic effects induced by leptin [4,5]. We previously reported that 5-HT2C and 5-HT1B receptor gene expression increased in hyperphagic A^y mice compared with wild-type mice, and that pharmacologic activation of 5-HT2C and 5-HT1B receptors suppressed food intake and body weight gain in hyperphagic A^y mice [6].

Serotonin (5-hydroxytryptamine; 5-HT) 2A receptors contribute to effects of 5-HT on platelet aggregation and vascular smooth muscle cell proliferation that lead to vascular occlusion at the site of vascular injury [7]. Sarpogrelate, a 5-HT2A receptor antagonist, has antiplatelet and antithrombotic effects and is clinically prescribed for the treatment with atherosclerosis and cardiovascular disease [8–11]. In addition, sarpogrelate in combination with antidiabetic agents reportedly increase plasma levels of adiponectin, an adipokine, in diabetic patients with arteriosclerosis obliterans [12]. 5-HT2A receptors are also located in the central nervous system including the hypothalamus [13,14]. The involvement of hypothalamic 5-HT2A receptors in the regulation of feeding, obesity, plasma adiponectin levels, and the expression of hypothalamic neuropeptide genes that are involved in regulating feeding and energy homeostasis, however, remains to be resolved.

In the present study, we examined the effects of sarpogrelate on appetite, and on the gene expression of hypothalamic neuropeptides that are involved in the regulation of feeding in C57BL6J mice. We also investigated alterations of hypothalamic 5-HT2A receptor gene expression, and the

* Corresponding author. Fax: +81 22 717 7612.
E-mail address: knonogaki-tky@umin.ac.jp (K. Nonogaki).

0006-291X/$ - see front matter © 2006 Elsevier Inc. All rights reserved.
doi:10.1016/j.bbrc.2006.10.173

effects of sarpogrelate on food intake, body weight, blood glucose levels, and plasma adiponectin levels in A^y mice and wild-type mice matched for age.

Materials and methods

Animals and drug treatment. Four-week-old male C57BL/6J mice, A^y mice, and wild-type mice (KK background) were purchased from Japan CLEA. Mice were individually housed in cages with free access to water and chow pellets in a light- (lights on: 8:00 h, lights off: 20:00 h) and temperature- (20–22 °C) controlled environment. Animals were acclimatized to the laboratory environment for 1 week before the experiment. Drugs were administered between 10:00 and 12:00 as described previously [6,15]. Sarpogrelate hydrochloride (a blood–brain barrier penetrating 5-HT2A receptor antagonist) was supplied by Mitsubishi Pharma (Osaka, Japan). Sarpogrelate was dissolved in saline.

In the first experiment, 5-week-old C57BL6J mice were deprived of food for 23 h. The following morning, the animals were injected intraperitoneally with saline or sarpogrelate (3–60 mg/kg) 30 min prior to food presentation. Intake of chow pellets was measured every hour for the next 1 or 4 h.

In the second experiment, 5-week-old C57BL6J mice were intraperitoneally injected with saline or sarpogrelate (30 mg/kg). Animals were not fed chow pellets after administration. Sixty minutes later, the hypothalamus was removed for RNA extraction.

In the third experiment, 5-week- and 8-week-old male A^y mice and wild-type littermates in fed state were decapitated and the prefrontal cortex and hypothalamus were removed for RNA extraction. The decapitation was done between 10:00 and 12:00.

In the fourth experiment, 8-week-old obese A^y mice and wild-type littermates were intraperitoneally injected with saline or sarpogrelate (30 mg/kg) twice daily (at 10:00 and 18:00) for 3 d. Daily food intake and body weight were measured. The animals were decapitated and blood was collected for measurement of blood glucose and adiponectin levels at 3 d. Whole blood was mixed with EDTA-2Na (2 mg/ml) to determine plasma adiponectin levels.

Finally, 5-week-old wild-type littermates were intraperitoneally injected with saline or sarpogrelate (30 mg/kg). Animals were not fed chow pellets after administration. Sixty and 120 min later, the animals were decapitated and blood was collected for measurement of adiponectin levels.

The dose of sarpogrelate dihydrochloride (30 mg/kg) was based on the evidence that sarpogrelate suppresses platelet aggregation and formation of platelet-rich thrombus by blockade of 5-HT2A receptors in rodents [8].

The animal studies were conducted under protocols in accordance with the institutional guidelines for animal experiments at Tohoku University Graduate School of Medicine.

Real-time quantitative RT-PCR. Total RNA was isolated from mouse hypothalamic tissue using the RNeasy Midi kit (Qiagen, Hilden, Germany) according to the manufacturer's directions, and cDNA synthesis was performed using a Super Script III First-Strand Synthesis System for RT-PCR Kit (Invitrogen, Rockville, MD) using 1 μg total RNA. cDNA synthesized from total RNA was evaluated in a real-time polymerase chain reaction (PCR) quantitative system (Light Cycler Quick System 350S; Roche Diagnostics, Mannheim, Germany). The primers used were as follows: for mouse pro-opiomelanocortin (POMC), sense, 5′-ATA GAT GTG TGG AGC TGG TG-3′, antisense, 5′-GGC TGT TCA TCT CCG TTG-3′; for mouse cocaine- and amphetamine-regulated transcript (CART), sense, 5′-CTG GAC ATC TAC TCT GCC GTG G-3′, antisense, 5′-GTT CCT CGG GGA CAG TCA CAC AGC-3′; for mouse corticotropin releasing hormone (CRH), sense, 5′-CCG GGC AGA GCA GTT AGC-3′, antisense, 5′-CAA CAT TTC ATT TCC CGA TAA TCT C-3′, for mouse neuropeptide Y (NPY), sense, 5′-GCT TGA AGA CCC TTC CAT TGG TG-3′, antisense, 5′-GGC GGA GTC CAG CCT AGT GG-3′; for mouse 5-HT1B receptor, sense, 5′-TGC CTG CTG GTT TCA CAT-3′, 5′-ATA GAT GTG TGG AGC TGG TG-3′, antisense, 5′-GCG CAC TTA AAG CGT ATC A-3′; for mouse 5-HT2A receptor, sense, 5′-TTC AGT GCC AGT ACA AGG AG-3′, antisense, 5′-GAG TGT TGG TTC CCT AGT GTA A-3′; for mouse 5-HT2C receptor, sense, 5′-CTG AGG GAC GAA AGC AAA G-3′, antisense, 5′-CAC ATA GCC AAT CCA AAC AAA C-3′; and for mouse β-actin, sense, 5′-TTG TAA CCA ACT GGG ACG ATA TGG-3′, antisense, 5′-GAT CTT GAT CTT CAT GGT GCT AGG-3′. The relative amount of mRNA was calculated with β-actin mRNA as the invariant control. The data are shown as the fold change of the mean value of the control group, which received saline.

Blood chemistries. Blood glucose levels were measured by glucose strips (Freestyle, Kissei Blood glucose monitoring system, Kissei, Japan). Plasma adiponectin levels were measured by enzyme-linked immunosorbent assay (mouse/rat Adiponectin ELISA kit, Ootsuka Pharmaceutical Inc., Japan).

Statistical methods. Data are presented as mean values ± SEM. Statistical significance of differences between two groups was determined using Student's *t*-test. Comparisons among more than two groups were done by analysis of variance using Bonferroni's correction for multiple comparisons. A P value of less than 0.05 was considered statistically significant.

Results and discussion

Dose–response effects and time course of the effects of sarpogrelate on food intake

To determine the dose–response effects of sarpogrelate on food intake, we examined food intake after the administration of sarpogrelate (3–60 mg/kg) or saline in C57BL6J mice. Administration of sarpogrelate (20–60 mg/kg) significantly reduced food intake in C57BL6J mice (to approximately 50–60% that of saline controls). Lower doses of sarpogrelate (3–10 mg/kg) had no effect on food intake during a 1-h feeding period after a 23-h fast in C57BL6J mice (Fig. 1A). To further determine the time course of the effects of sarpogrelate on food intake, we examined food intake

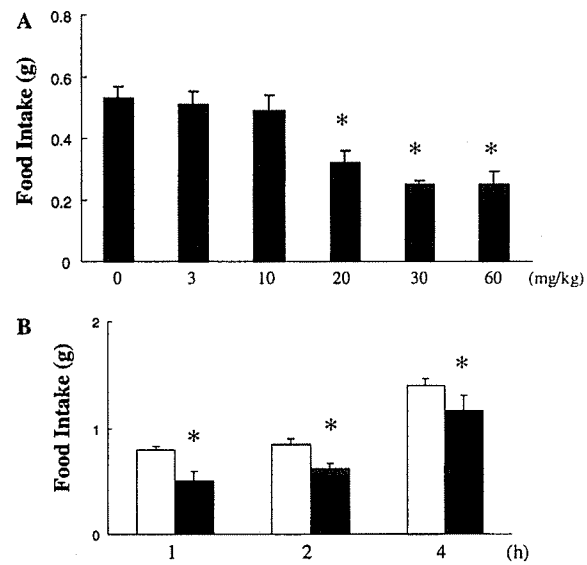

Fig. 1. Dose–response effects of sarpogrelate on food intake (A), time course of the effects of sarpogrelate (30 mg/kg) on food intake (B) in C57BL6J mice. After a 23-h fast, mice were intraperitoneally injected with sarpogrelate or saline. Open bar, saline; filled bars, sarpogrelate (3–60 mg/kg). Values are means ± SEM of 7–8 animals. $^*P < 0.05$ versus saline.

after administration of sarpogrelate (30 mg/kg) or saline in C57BL6J mice. The doses of sarpogrelate to induce anorexic effects were within the range to induce antiplatelet and antithrombotic effects in rodents [8]. In addition, the anorexic effects of sarpogrelate (30 mg/kg) were sustained for 4 h (Fig. 1B).

Effects of sarpogrelate on the expression of hypothalamic POMC, CART, CRH, NPY, 5-HT2C receptor, and 5-HT1B receptor genes

To determine the central mechanisms of the anorexic effects induced by sarpogrelate, we examined the expression of hypothalamic anorexigenic peptides. Sarpogrelate significantly increased hypothalamic POMC, CART, and CRH mRNA levels compared with saline controls (3-fold, 2-fold, and 1.9-fold compared with saline controls, respectively) at 1 h (Fig. 2). Interestingly, sarpogrelate also significantly increased hypothalamic 5-HT2C and 5-HT1B receptor mRNA levels compared with saline controls (2-fold, and 1.7-fold compared with saline controls, respectively) at 1 h. In addition, sarpogrelate slightly but significantly increased hypothalamic NPY mRNA levels (1.3-fold compared with saline controls) at 1 h (Fig. 2).

Hypothalamic 5-HT2A receptor gene expression in A^y mice

Hypothalamic 5-HT2A receptor mRNA levels were significantly increased in 8-week-old obese A^y mice compared with wild-type mice (1.4-fold compared with saline controls), whereas there were no significant differences in hypothalamic 5-HT2A receptor mRNA levels in 5-week-old A^y mice and wild-type mice (Fig. 3). 5-HT2A receptor mRNA levels in the prefrontal cortex were not significantly changed in A^y mice compared with wild-type mice matched for age (data not shown).

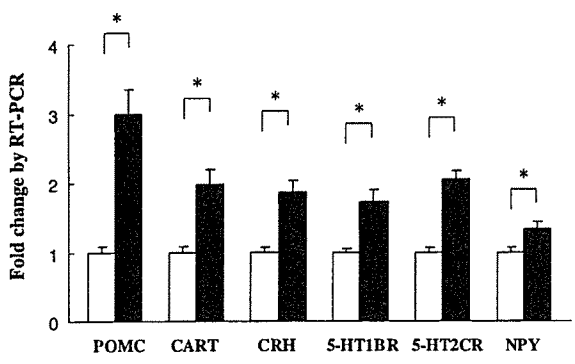

Fig. 2. Effects of sarpogrelate on hypothalamic POMC, CART, CRH, 5-HT2C receptor, and 5-HT1B receptor mRNA levels in C57BL6J mice. Mice were intraperitoneally injected with sarpogrelate or saline. Open bar, saline; filled bars, sarpogrelate (30 mg/kg). Each column and bar represents the means ± SEM of 5–6 mice. POMC, pro-opiomelanocortin; CART, cocaine- and amphetamine-regulated transcript; CRH, corticotropin releasing hormone, sarpo, sarpogrelate. $^*P < 0.05$.

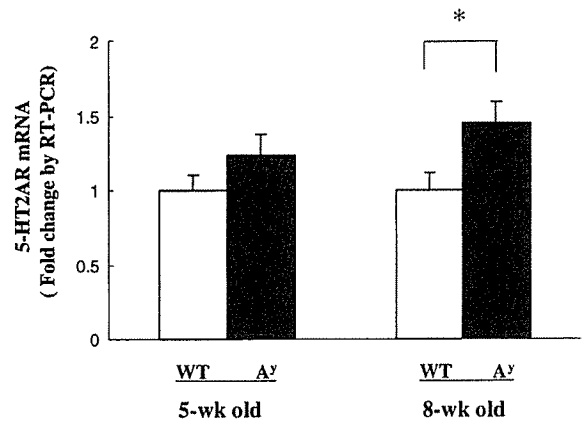

Fig. 3. Hypothalamic 5-HT2A receptor mRNA levels in A^y mice and wild-type mice (5-week-old mice; A, 8-week-old mice; B). Open bar, wild-type mice; filled bars, A^y mice. Each column and bar represents mean ± SEM of 5–6 mice. $^*P < 0.05$.

Effects of sarpogrelate on food intake, body weight, and plasma adiponectin levels in A^y mice

Eight-week-old A^y mice and wild-type mice received sarpogrelate (30 mg/kg) or saline twice daily for three consecutive days. Sarpogrelate administration reduced food intake and body weight in both A^y mice and wild-type mice at 2 d and 3 d (Fig. 4A–D). Sarpogrelate-induced decreases in food intake and body weight were greater in A^y mice than wild-type mice. In addition, sarpogrelate remarkably reduced hyperglycemia in A^y mice while having no significant effects on blood glucose levels in wild-type mice (Fig. 4E). There were no differences in plasma adiponectin levels between treatment with sarpogrelate (30 mg/kg) and saline in A^y mice and wild-type mice (Fig. 4F). Next, we examined the acute effects of sarpogrelate on plasma adiponectin levels in wild-type mice. Sarpogrelate (30 mg/kg) significantly decreased plasma adiponectin levels compared with saline controls at 1 h in wild-type mice (saline controls, 12.5 ± 0.4 μg/ml; sarpogrelate treatment group, 10.5 ± 0.7 μg/ml; $n = 7$ for each group, $P < 0.05$), but did not affect at 2 h (saline controls, 11.7 ± 0.7 μg/ml; sarpogrelate treatment group, 10.9 ± 0.4 μg/ml; $n = 6$ and 7 for each group, $P = 0.34$).

The results of the present study demonstrate that hypothalamic 5-HT2A receptor gene expression was increased in association with obesity in A^y mice compared with wild-type mice, and pharmacologic inactivation of 5-HT2A receptors suppressed hyperphagia and body weight gain, leading to decreased blood glucose levels in obese A^y mice. Overfeeding leads to hyperglycemia in A^y mice, because restricted feeding attenuates hyperglycemia in A^y mice [6]. Hypothalamic 5-HT2A receptors might therefore be involved in the development of obesity and diabetes in A^y mice. We previously reported that 5-HT2C and 5-HT1B receptor gene expression was increased in non-obese hyperphagic A^y mice and pharmacologic activation of 5-HT2C

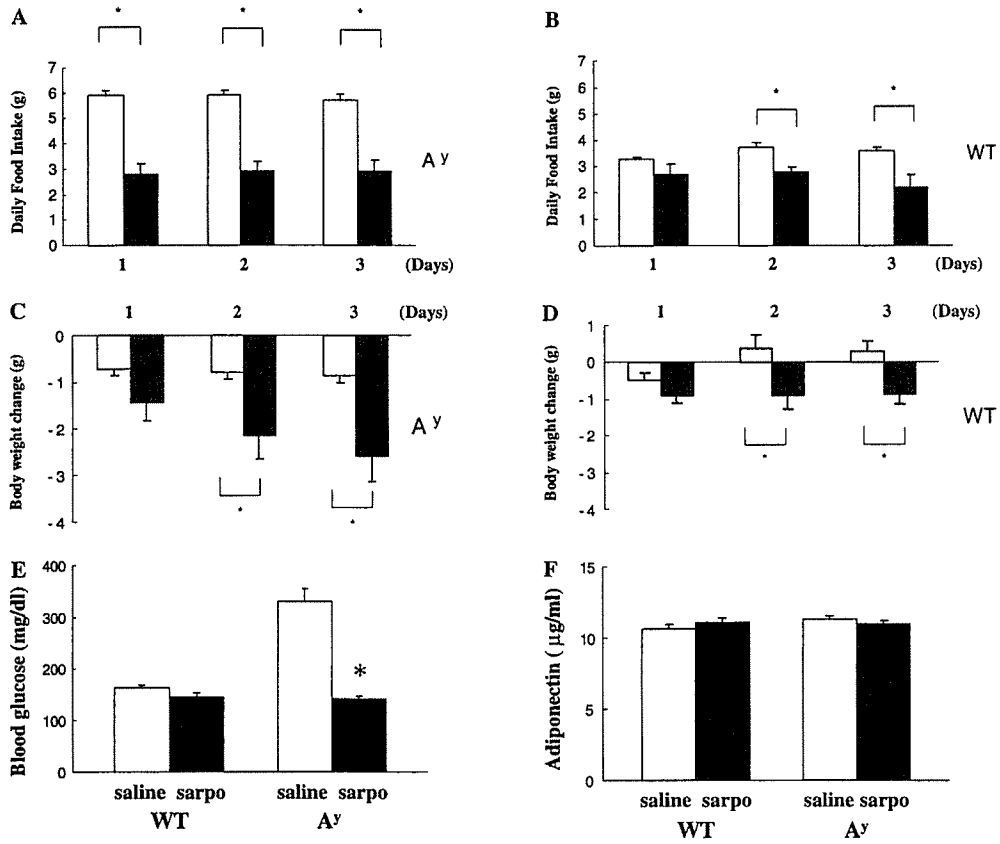

Fig. 4. Effects of chronic administered sarpogrelate on food intake (A,B), body weight (C,D), blood glucose levels (E), and plasma adiponectin levels (F) in 8-week-old A^y mice and wild-type mice. Each column and bar represents mean ± SEM of 7–9 mice. Basal body weight: WT saline controls (open bars), 30.6 ± 0.3 g; WT sarpogrelate treatment group (filled bars), 30.0 ± 0.7 g; A^y saline controls (open bars), 40.8 ± 1.0 g; A^y sarpogrelate treatment group (filled bars), 39.5 ± 1.0 g; WT, wild-type. $^*P < 0.05$.

and/or 5-HT1B receptors suppressed feeding and body weight gain in A^y mice [6]. The increase in hypothalamic 5-HT2C and 5-HT1B receptor gene expression might therefore be a compensatory response to hyperphagia induced by the agouti peptide in A^y mice. Thus, hypothalamic 5-HT2A receptors and 5-HT2C/1B receptors might have a reciprocal role in the regulation of feeding and energy homeostasis.

The results of present study also demonstrates that sarpogrelate increased expression of hypothalamic POMC, CART, and CRH genes that are similar to those of mCPP and fenfluramine [15,16], which cause anorexic effects via 5-HT2C receptors and/or 5-HT1B receptors [17–21]. Moreover, sarpogrelate increased hypothalamic 5-HT2C and 5-HT1B receptor gene expression. These findings suggest that 5-HT2A receptors are likely to down-regulate POMC, CART, CRH, 5-HT2C, and 5-HT1B receptor gene expression in the hypothalamus. In addition to the inactivation of 5-HT2A receptors, sarpogrelate interacts with POMC neurons in the hypothalamus and could stimulate POMC neurons to release enough α-melanocyte stimulating hormone to overcome agouti blockade of MC receptors, because A^y mice are sensitive to MC agonist-induced feeding suppression [2]. Moreover, CART might contribute to the sarpogrelate-induced feeding suppression in A^y mice; possibly, because CART and MC neurons do not share a downstream pathway [22,23]. These pathways might contribute to the mechanisms of sarpogrelate-induced feeding suppression.

Adiponectin is an adipokine that is secreted by white adipose tissue and directly sensitizes the body to insulin [24]. Hypoadiponectinemia has been indicated as a causal factor in insulin resistance and the metabolic syndrome [24]. Sarpogrelate in combination with antidiabetic agents reportedly increase plasma adiponectin levels in diabetic patients with arteriosclerosis obliterans [12]. Our results of the present study demonstrate that chronic treatment with sarpogrelate alone had no effects on plasma adiponectin levels in 8-week-old A^y mice and wild-type mice while it is suppressed overfeeding, body weight gain, and hyperglycemia in 8-week-old A^y mice. The present results might support our previous clinical findings that plasma adiponectin levels are not related to overweight and glycemic control in type 2 diabetes subjects [25]. The stimulatory effects of sarpogrelate on adiponectin might therefore require antidiabetic agents. Otherwise, the stimulatory effects of sarpogrelate on adiponectin might require low

plasma adiponectin levels, because 8-week-old A^y mice did not have decreased plasma adiponectin levels compared with wild-type age-matched mice.

In summary, these results suggest that hypothalamic 5-HT2A receptor gene expression is increased in association with obesity in A^y mice, and pharmacologic inactivation of 5-HT2A receptors suppresses overfeeding and obesity, which leads to the improvement of diabetes in A^y mice. Sarpogrelate induces appetite suppressing effects and increases hypothalamic POMC, CART, CRH, 5-HT2C, and 5-HT1B receptor gene expression while having no stimulatory effects on plasma adiponectin levels in mice.

Acknowledgments

This work was supported by a Grant-in-Aid for Scientific Research (C2) and Human Science Research (KH21016).

References

[1] D. Lu, D. Willard, I.R. Patel, S. Kadwell, L. Overton, T. Kost, M. Luther, W. Chen, R.P. Woychik, W.O. Wilkison, R.D. Cone, Agouti protein is an antagonist of the elanocyte-stimulating-hormone receptor, Nature 371 (1994) 799–802.

[2] W. Fan, B.A. Boston, R.A. Kesterson, V.J. Hruby, R.D. Cone, Role of melanocortinergic neurons in feeding and the agouti obesity syndrome, Nature 385 (1997) 165–168.

[3] K. Ebihara, Y. Ogawa, G. Katsuura, Y. Numata, H. Masuzaki, N. Satoh, M. Tamaki, T. Yoshioka, M. Hayase, N. Matsuoka, M. Aizawa-Abe, Y. Yoshimasa, K. Nakao, Involvement of agouti-related protein. an endogenous antagonist of hypothalamic melanocortin receptor, in leptin action, Diabetes 48 (1999) 2028–2033.

[4] B.A. Boston, K.M. Blaydon, J. Varnerin, R.D. Cone, Independent and additive effects of central POMC and leptin pathways on murine obesity, Science 278 (1997) 1641–1644.

[5] B.D. Wilson, D. Bagnol, C.B. Kaelin, M.M. Ollmann, I. Gantz, S.J. Watson, G.S. Barsh, Physiological and anatomical circuitry between Agouti-related protein and leptin signaling, Endocrinology 140 (1999) 2387–2397.

[6] K. Nonogaki, K. Nozue, Y. Oka. Hyperphagia alters expression of hypothalamic 5-HT2C and 5-HT1B receptor genes and plasma desacyl ghrelin levels in A^y mice, Endocrinology, in press.

[7] C. Ullmer, K. Schmuck, H.O. Kalkman, H. Lubbert, Expression of serotonin receptor mRNAs in blood vessels, FEBS Lett. 370 (1995) 215–221.

[8] H. Hara, A. Kitajima, H. Shimada, Y. Tamano, Antithrombotic effects of MCI-9094, a new antiplatelet agent on experimental thrombosis models, Thromb. Haemost. 66 (1991) 484–488.

[9] X. Tobesseda, N. Mealy, Sarpogrelate hydrochloride: a peripheral serotonin 5-HT2 receptor antagonist with platelet anti aggregatory properties, Drugs Today 30 (1999) 43–48.

[10] H.K. Saini, N. Takeda, R.K. Goyal, H. Kumamoto, A.S. Arneja, N.S. Dhalla, Theraprutic potentials of Sarpogrelate in cardiovascular disease, Cardiovas. Drug Rev. 22 (2004) 27–54.

[11] T. Nagamoto, M. Rashid, H.A. Muntasir, T. Komiyama, Functions of 5-HT2A receptor and its antagonists in the cardiovascular system, Pharmacol. Ther. 104 (2004) 59–81.

[12] J. Yamakawa, T. Takahashi, T. Itoh, K. Kusaka, K. Kawaura, X.Q. Wang, T. Kanda, A novel serotonin blocker, sarpogrelate, increases circulating adiponectin levels in diabetic patients with arteriosclerosis obliterans, Diabetes Care 26 (2003) 2477–2478.

[13] N.M. Barnes, T. Sharp, A review of central 5-HT receptors and their function, Neuropharmacology 38 (1999) 1083–1152.

[14] X.F. Huang, M. Han, X. Huang, K. Zavitsanou, C. Deng, Olanzapine differentially affects 5-HT2A and 2C receptor mRNA expression in the rat brain, Behav. Brain Res. 171 (2006) 355–362.

[15] K. Nonogaki, K. Ohashi-Nozue, Y. Oka, A negative feedback system between brain serotonin systems and plasma active ghrelin levels in mice, Biochem. Biophys. Res. Commun. 341 (2006) 703–707.

[16] N. Laflamme, S. Bovetto, D. Richard, S. Rivest, Effect of dexfenfluramine on the transcriptional activation of CRF and its type 1 receptor within the paraventricular nucleus of the rat hypothalamus, Br. J. Pharmacol. 117 (1996) 1021–1034.

[17] L.H. Tecott, L.M. Sun, S.F. Akana, A.M. Strack, D.H. Lowenstein, M.F. Dallman, D. Julius, Eating disorder and epilepsy in mice lacking 5-HT2C serotonin receptors, Nature 374 (1995) 542–546.

[18] S.P. Vickers, P.G. Clifton, C.T. Dourish, L.H. Tecott, Reduced satiating effect of d-fenfluramine in serotonin 5-HT(2C) receptor mutant mice, Psychopharmacology 143 (1999) 309–314.

[19] S.P. Vickers, C.T. Dourish, G.A. Kennett, Evidence that hypophagia induced by d-fenfluramine and d-norfenfluramine in the rat is mediated by 5-HT2C receptors, Neuropharmacology 41 (2001) 200–209.

[20] J.J. Lucas, A. Yamamoto, K. Scearce-Levie, F. Saudou, R. Hen, Absence of fenfluramine-induced anorexia and reduced c-Fos induction in the hypothalamus and central amygdaloid complex of serotonin 1B receptor knock-out mice, J. Neurosci. 18 (1998) 5537–5544.

[21] M.D. Lee, E.M. Somerville, G.A. Kennett, C.T. Dourish, P.G. Clifton, Reduced hypophagic effects of d-fenfluramine and the 5-HT2C receptor agonist mCPP in 5-HT1B receptor knockout mice, Psychopharmacology 176 (2004) 39–49.

[22] C. Broberger, Hypothalamic cocaine- and amphetamine-regulated transcript (CART) neurons: histochemical relationship to thyrotropin-releasing hormone, melanin concentrating hormone, orexin/hypocretin and neuropeptide Y, Brain Res. 848 (1999) 101–113.

[23] C.F. Elias, C.E. Lee, J.F. Kelly, R.S. Ahima, M. Kuhar, C.B. Saper, J.K. Elmquist, Characterization of CART neurons in the rat and human hypothalamus, J. Com. Neurol. 432 (2001) 1–19.

[24] T. Kadowaki, T. Yamauchi, N. Kubota, K. Hara, K. Ueki, K. Tobe, Adiponectin and adiponectin receptors in insulin resistance, diabetes, and the metabolic syndrome, J. Clin. Invest. 116 (2006) 1784–1792.

[25] K. Nnoogaki, H. Kumano, Y. Ootsuka, A. Takeuchi, N. Nonogaki, T. Kuboki, Clinical worth of adiponectin levels in obesity and glycemic control of Japanese type 2 diabetic patients, Diabetes Care 26 (2003) 3198.

Myosin motor Myo1c and its receptor NEMO/IKK-γ promote TNF-α–induced serine^{307} phosphorylation of IRS-1

Yoshitaka Nakamori,[1] Masahiro Emoto,[1] Naofumi Fukuda,[1] Akihiko Taguchi,[1] Shigeru Okuya,[1] Michiko Tajiri,[2,3] Makoto Miyagishi,[4] Kazunari Taira,[4] Yoshinao Wada,[2,3] and Yukio Tanizawa[1]

[1]Division of Molecular Analysis of Human Disorders, Department of Bio-Signal Analysis, Yamaguchi University Graduate School of Medicine, Ube 755-8505, Japan
[2]Core Research for Evolution Science and Technology, Japan Science and Technology Agency, Saitama 332-0012, Japan
[3]Department of Molecular Medicine, Osaka Medical Center and Research Institute for Maternal and Child Health, Izumi, Osaka 594-1101, Japan
[4]Department of Chemistry and Biotechnology, University of Tokyo, Bunkyo-ku, Tokyo 113-8656, Japan

Tumor necrosis factor-α (TNF-α) signaling through the IκB kinase (IKK) complex attenuates insulin action via the phosphorylation of insulin receptor substrate 1 (IRS-1) at Ser^{307}. However, the precise molecular mechanism by which the IKK complex phosphorylates IRS-1 is unknown. In this study, we report nuclear factor κB essential modulator (NEMO)/IKK-γ subunit accumulation in membrane ruffles followed by an interaction with IRS-1. This intracellular trafficking of NEMO requires insulin, an intact actin cytoskeletal network, and the motor protein Myo1c. Increased Myo1c expression enhanced the NEMO–IRS-1 interaction, which is essential for TNF-α–induced phosphorylation of Ser^{307}–IRS-1. In contrast, dominant inhibitory Myo1c cargo domain expression diminished this interaction and inhibited IRS-1 phosphorylation. NEMO expression also enhanced TNF-α–induced Ser^{307}–IRS-1 phosphorylation and inhibited glucose uptake. In contrast, a deletion mutant of NEMO lacking the IKK-β–binding domain or silencing NEMO blocked the TNF-α signal. Thus, motor protein Myo1c and its receptor protein NEMO act cooperatively to form the IKK–IRS-1 complex and function in TNF-α–induced insulin resistance.

Introduction

Insulin resistance, a condition in which the cells become resistant to the effects of insulin, is a major risk factor for type 2 diabetes as well as hypertension, dyslipidemia, and atherosclerosis (Reaven, 1988). Despite several investigations, the molecular mechanism underlying insulin resistance has not been adequately clarified. TNF-α is an adipocytokine and induces insulin resistance (Hotamisligil et al., 1993). A TNF-α signal results in the phosphorylation of Ser^{307} of insulin receptor (IR) substrate 1 (IRS-1), in turn attenuating the metabolic insulin signal (Kanety et al., 1995). Many serine kinases such as JNK, glycogen synthase kinase 3, and mammalian target of rapamycin have been reported to phosphorylate serine residues of IRS-1 (Gao et al., 2002). However, the serine kinase that precisely regulates metabolic insulin action is unclear.

After the first report of type 2 diabetes being successfully treated with high-dose salicylate in 1901 (Williamson and Lond, 1901), numerous attempts have been made to identify the target molecules of salicylate. In 1998, salicylate was reported to be a strong inhibitor of the kinase activity of IκB kinase (IKK) β (Yin et al., 1998). Since then, studies have focused on the IKK complex as a critical molecule for the development of insulin resistance (Yuan et al., 2001). The IKK complex consists of two catalytic subunits, IKK-α and IKK-β, and one scaffold subunit designated nuclear factor κB essential modulator (NEMO)/IKK-γ (DiDonato et al., 1997; Nakano et al., 1998; Yamaoka et al., 1998). Among these subunits, IKK-β is a key insulin resistance molecule, as demonstrated by a study using the IKK-β knockout mouse (Kim et al., 2001). A recent study showed the IKK complex to phosphorylate IRS-1 at Ser^{307}, which is associated with TNF-α stimulation and diminished insulin signaling (Gao et al., 2002). However, whether IKK-β itself physically binds to IRS-1 is uncertain. Furthermore, the role of NEMO is also unclear.

Myo1c is a motor protein that is classified as an unconventional myosin I. This class of myosins is widely distributed, having been identified in organisms from yeast to human. In adipocytes, Myo1c reportedly facilitates the recycling of vesicles containing glucose transporter 4 (Bose et al., 2002). However, little is known about the molecular mechanisms regulating motor Myo1c–cargo interactions.

Correspondence to Masahiro Emoto: emotom@yamaguchi-u.ac.jp

Abbreviations used in this paper: eGFP, enhanced GFP; IKK, IκB kinase; IR, insulin receptor; IRS-1, IR substrate 1; NEMO, nuclear factor κB essential modulator; shRNA, short hairpin RNA; WT, wild type.

The online version of this article contains supplemental material.

The Journal of Cell Biology, Vol. 173, No. 5, June 5, 2006 665–671
http://www.jcb.org/cgi/doi/10.1083/jcb.200601065

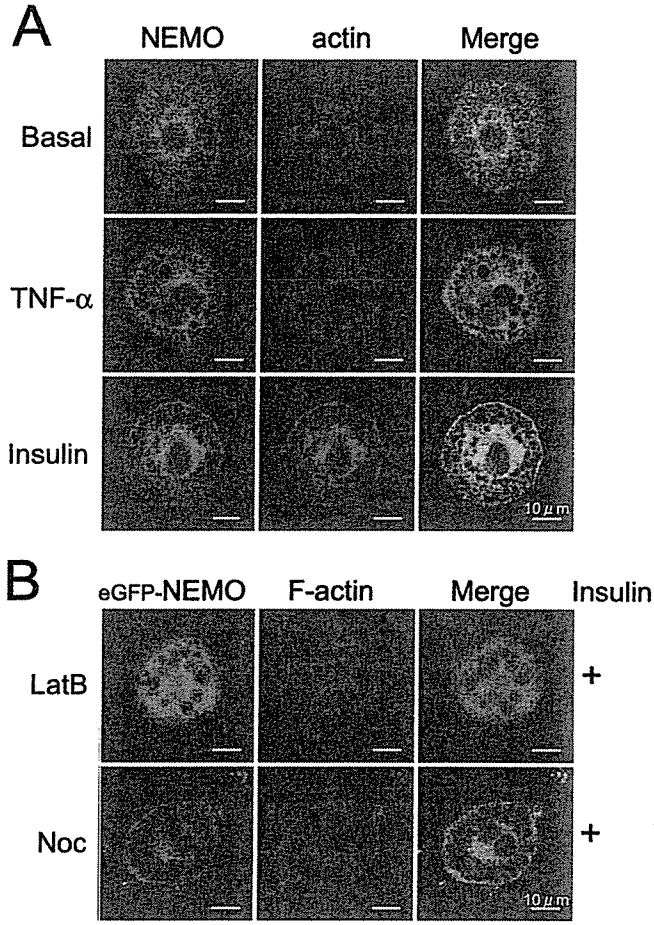

Figure 1. **Intracellular localization of NEMO in 3T3-L1 adipocytes.** Differentiated 3T3-L1 adipocytes (A) or adipocytes expressing eGFP-NEMO (B) were serum starved and either left untreated (A) or were pretreated with 5 μM latrunculin B (LatB) or 30 μM nocodazole (Noc) for 60 min (B). They were then incubated with 20 ng/ml TNF-α or 100 nM insulin for 15 min at 37°C. The cells were fixed, and F-actin was visualized by AlexaFluor596-phalloidin.

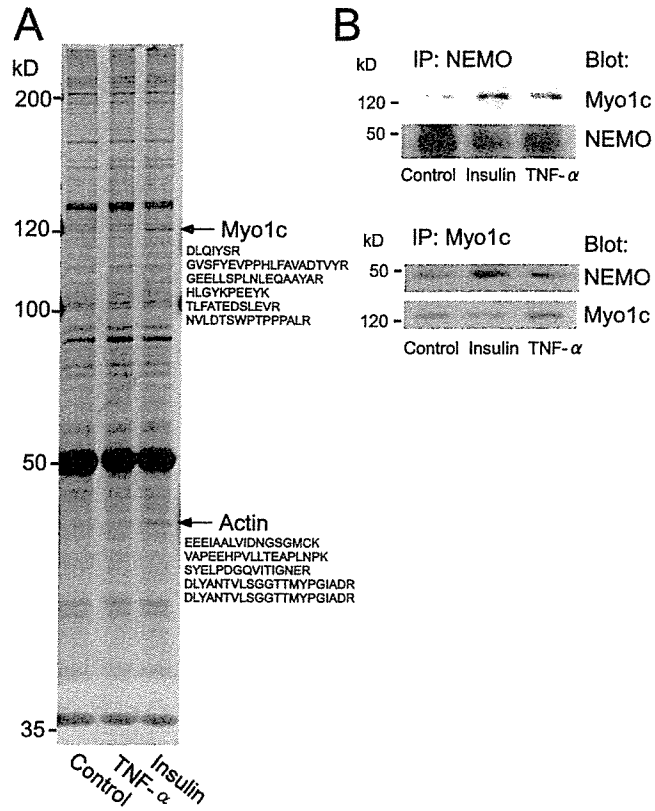

Figure 2. **Insulin promotes the interaction between NEMO and Myo1c.** (A) 3T3-L1 adipocytes expressing myc-tagged WT NEMO were serum starved and stimulated with 100 nM insulin or 20 ng/ml TNF-α for 20 min at 37°C. NEMO-binding proteins were immunoprecipitated with anti-myc antibody, separated by SDS-PAGE, and visualized by silver staining. Bands were proteolytically digested and analyzed by mass spectrometry. Myo1c and actin (arrows) were identified. (B) 3T3-L1 adipocytes were serum starved for 2 h and treated with 100 nM insulin or 20 ng/ml TNF-α for 20 min at 37°C. The NEMO–Myo1c interaction was determined by immunoprecipitation using anti-NEMO or anti-Myo1c antibodies.

We investigated the formation of the functional complex of signaling molecules containing IKKs and IRS-1 in response to insulin. We found that NEMO functions as a motor receptor, whereas Myo1c and the actin cytoskeleton facilitate translocation of the IKK complex to membrane ruffles or to the vicinity of IRS-1. This interaction between IKKs and IRS-1 is essential for TNF-α–induced phosphorylation of IRS-1 at Ser^{307}, which results in the inhibition of glucose uptake. Our present results suggest a novel mechanism whereby Myo1c–NEMO-mediated signaling complex formation plays a role in TNF-α–induced insulin resistance.

Results and discussion

NEMO translocates to membrane ruffles in response to insulin

Researchers have reported that IKK-β is crucial for TNF-α–induced IRS-1 serine phosphorylation (Gao et al., 2002; de Alvaro et al., 2004). However, the role of the NEMO/IKK-γ subunit is poorly understood. We first examined the intracellular localization of NEMO in differentiated 3T3-L1 adipocytes using anti-NEMO antibody. As shown in Fig. 1 A, NEMO results in a fine punctate or granular appearance throughout the cytoplasm under basal and TNF-α–treated conditions. In contrast, the addition of insulin to culture adipocytes yields the rapid translocation of NEMO to the cell periphery, especially in membrane ruffles visualized by staining with AlexaFluor596-phalloidin. This translocation is similar to that seen in other cell types (Weil et al., 2003). Interestingly, treatment with the actin depolymerizer latrunculin B inhibited NEMO translocation, whereas the microtubule disrupter nocodazole did not (Fig. 1 B). These data suggest that insulin stimulates the accumulation of NEMO at membrane ruffles through the cortical actin network.

Identification of motor protein Myo1c as a NEMO-binding partner

Because NEMO has neither an actin-binding motif nor a membrane-targeting domain, we attempted to identify NEMO-binding proteins using mass spectrometry. 3T3-L1 adipocytes were infected with an adenovirus vector containing myc-tagged full-length NEMO and were treated with 20 ng/ml TNF-α or 100 nM insulin for 20 min. The cell lysates were immunoprecipitated with anti-myc antibody. The precipitates were

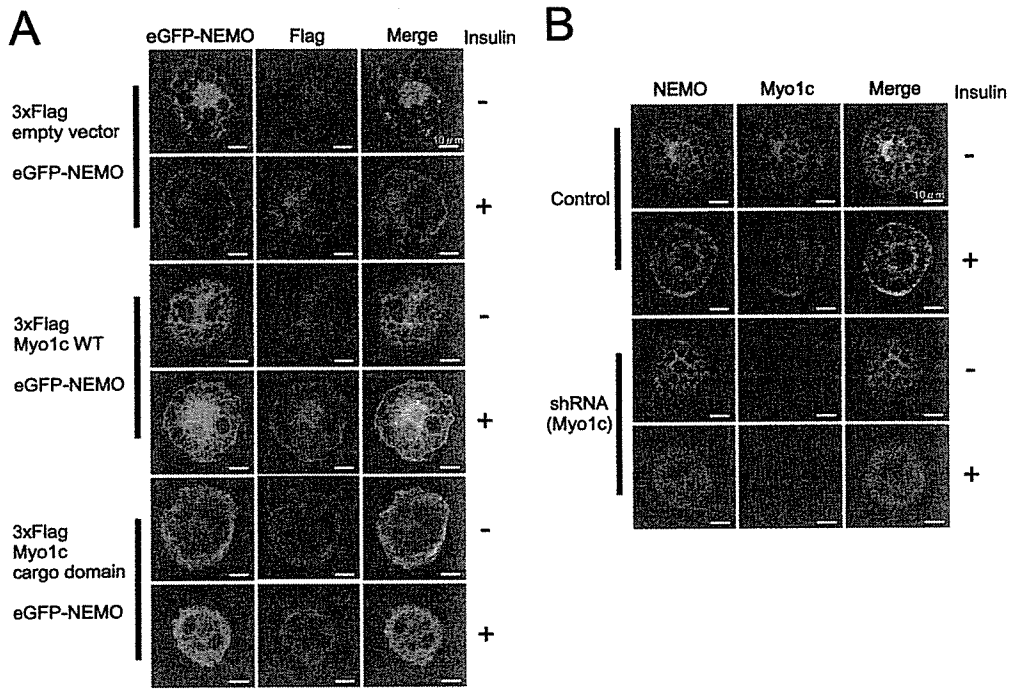

Figure 3. **Effect of Myo1c expression on the intracellular localization of NEMO.** 3T3-L1 adipocytes were coexpressed with eGFP-NEMO and WT Myo1c or the Myo1c cargo domain (A) or were infected with adenovirus encoding shRNA (Myo1c) or vector alone. After 2 h of serum starvation, the cells were stimulated with or without 100 nM insulin for 20 min at 37°C, stained with anti-Flag antibody followed by Cy3-labeled secondary antibody (A) or anti-NEMO antibody and anti-Myo1c antibody followed by FITC and Cy3-labeled secondary antibodies (B), and were observed by confocal microscopy.

resolved by SDS-PAGE and visualized with silver staining. With in-gel digestion followed by peptide mass fingerprinting, we identified two candidate proteins, Myo1c and actin, showing increased binding to NEMO in the presence of insulin (Fig. 2 A, arrowheads). A series of experiments were performed to confirm the interaction between NEMO and Myo1c. We first examined endogenous protein–protein interactions by immunoprecipitation using polyclonal anti-NEMO– and polyclonal anti-Myo1c–specific antibodies. As shown in Fig. 2 B, insulin treatment increased NEMO–Myo1c binding. We next confirmed this interaction using recombinant proteins in vitro. GST-tagged NEMO and His-tagged Myo1c were purified, mixed, and pulled down with each other. As shown in Fig. S1 (available at http://www.jcb.org/cgi/content/full/jcb.200601065/DC1), the interaction was easily detected by immunoblotting. These results suggest that NEMO and Myo1c interact directly in an insulin-dependent manner.

Myo1c conveys NEMO

Based on the results presented in Figs. 1 and 2, we hypothesized that the IKK complex containing NEMO is transported from the cytosol to membrane ruffles by Myo1c. To examine this possibility, we conducted experiments using the dominant inhibitory cargo domain of Myo1c. Overexpression of this cargo domain (residues 767–1,028) has been shown to result in the dominant inhibition of cargo binding (Bose et al., 2002). 3xFlag-tagged full-length Myo1c (wild type [WT]) or the dominant inhibitory cargo domain of Myo1c was cotransfected into culture adipocytes with enhanced GFP (eGFP)–tagged NEMO. In cells coexpressing Myo1c WT and eGFP-NEMO, NEMO showed marked translocation to membrane ruffles with insulin stimulation. Interestingly, Myo1c WT also accumulated in the membrane and enhanced Myo1c expression, resulting in the extensive formation of membrane ruffles (Fig. 3 A). In contrast, cells expressing Myo1c cargo domain and NEMO showed the marked inhibition of insulin-stimulated NEMO translocation. Similar inhibition of NEMO translocation was observed in Myo1c knockdown cells using adenovirus encoding short hairpin RNA (shRNA [Myo1c]; Fig. 3 B).

We observed the association between NEMO and Myo1c biochemically (Fig. 2). We also found that membrane targeting of NEMO requires a motor protein, Myo1c (Fig. 3). Collectively, the data indicate the scaffold protein NEMO to be transported to membrane ruffles by the motor protein Myo1c. These observations are consistent with our aforementioned hypothesis.

Myo1c promotes IRS-1–IKK interaction and mediates Ser^{307} phosphorylation on IRS-1

A recent study showed that IKKs interact with IRS-1 and interfere with insulin signaling (Gao et al., 2002). To confirm this interaction in culture adipocytes, we first examined the localization of endogenous NEMO and IRS-1 (Fig. 4 A) or Xpress-tagged NEMO and eGFP-tagged IRS-1 (Fig. 4, B and C). In the basal state, IRS-1 was present in the cytoplasm, whereas with insulin stimulation, IRS-1 and NEMO colocalized to discrete foci in the cytoplasm as well as membrane ruffles. These observations on the intracellular localization of IRS-1 were very similar to those described in a study by Luo et al. (2005). They reported a mechanism of IRS-1 signal down-regulation involving the formation of a sequestration complex containing IRS-1 in

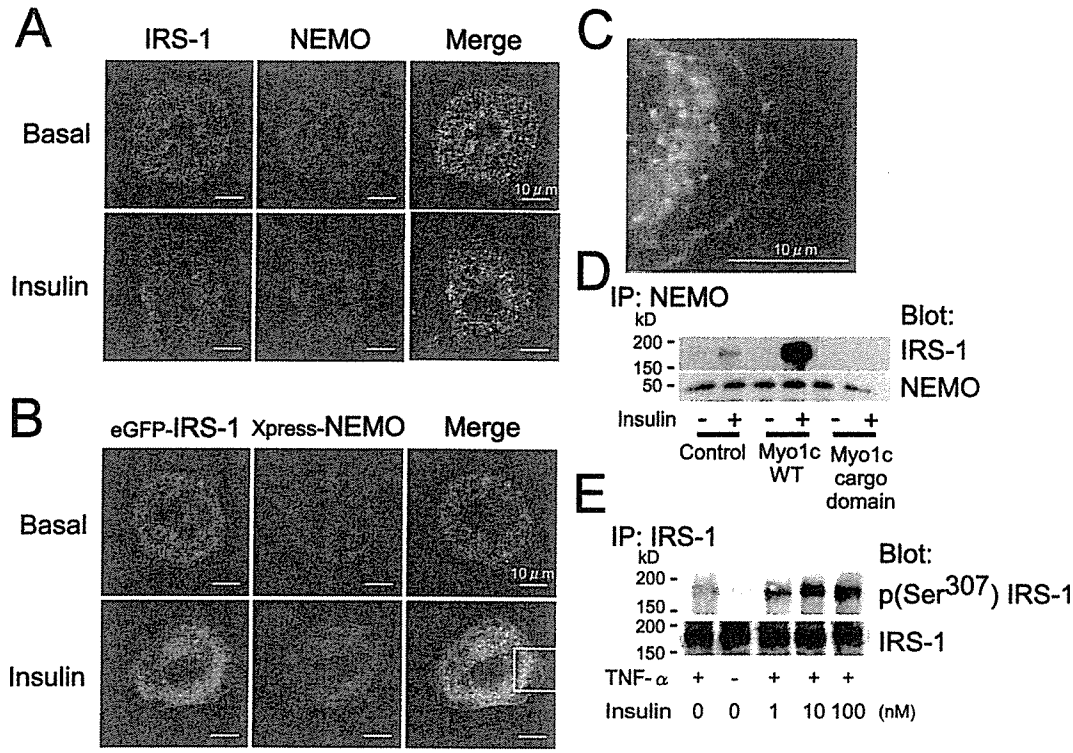

Figure 4. **Myo1c modulates IRS-1–NEMO interaction.** (A) 3T3-L1 adipocytes were serum starved for 2 h and stimulated with or without 100 nM insulin for 15 min at 37°C. Cells were fixed and stained with anti–IRS-1 and anti-NEMO antibody followed by FITC and Cy3-labeled secondary antibodies. (B) eGFP-tagged IRS-1 and Xpress-fused NEMO were coexpressed in 3T3-L1 adipocytes. After 2 h of serum starvation, the cells were stimulated with or without 100 nM insulin for 15 min and were then fixed. Expressed NEMO was visualized by anti-Xpress antibody and a Cy3-labeled second antibody. (C) High resolution view of the boxed area outlined in B. (D) 3T3-L1 adipocytes were infected with adenovirus encoding WT Myo1c and dominant inhibitory Myo1c. The cells were stimulated with or without 100 nM insulin for 15 min. The cell lysates were immunoprecipitated with anti-NEMO antibody, and precipitates were immunoblotted with anti–IRS-1 antibody. (E) 3T3-L1 adipocytes were left untreated or treated with 20 ng/ml TNF-α for 10 min and were incubated with various concentrations (1–100 nM) of insulin for 10 min at 37°C. The cells were lysed and immunoprecipitated by anti–IRS-1 antibody, and the precipitates were blotted with antiphospho-Ser^{307} IRS-1 and anti–IRS-1 antibody.

CHO-K1 cells. Interestingly, the large intracellular IRS-1 complexes (foci) appeared to be the negative regulatory machinery.

We next examined the direct interaction between endogenous IRS-1 and NEMO by immunoprecipitation (Fig. 4 D). Interestingly, the overexpression of Myo1c markedly increased this interaction. In contrast, cells overexpressing the dominant inhibitory cargo domain of Myo1c showed a diminished interaction. One interpretation of these findings is that Myo1c mediates the interaction by delivering NEMO to IRS-1. This explanation is supported by another set of experiments shown in Fig. S2 (A and B; available at http://www.jcb.org/cgi/content/full/jcb.200601065/DC1). These experiments focused on Myo1c–IKK-β and IRS-1–IKK-β associations. When NEMO was knocked down, the Myo1c–IKK-β interaction was disturbed. Similarly, the overexpression of ΔN-NEMO (detailed in the next section) diminished the IRS-1–IKK-β interaction. These results, combined with the data shown in Fig. 3, are consistent with our hypothesis that Myo1c transports the IKK complex via binding to NEMO.

Another interesting observation illustrated in Fig. 4 D was that insulin enhanced the association between IRS-1 and IKK-β. These data raise the possibility that insulin may assemble clusters of signaling molecules to facilitate the interaction between IKKs and IRS-1. To assess this possible new role of insulin, we performed two additional experiments. First, we observed IRS-1 Ser^{307} phosphorylation induced by TNF-α after treatment with various concentrations of insulin (Fig. 4 E). Although TNF-α–induced serine phosphorylation of IRS-1 was detected within 20 min even in the absence of insulin, a low concentration of insulin markedly enhanced TNF-α–induced Ser^{307} phosphorylation. These data are consistent with the results presented in Fig. 4 D. Next, we also observed Ser^{307} phosphorylation of IRS-1 in adipocytes expressing WT Myo1c and dominant inhibitory Myo1c. Overexpression of dominant inhibitory Myo1c diminished Ser^{307} phosphorylation of IRS-1 (Fig. S3 A, available at http://www.jcb.org/cgi/content/full/jcb.200601065/DC1). These results show that Myo1c promotes the interaction between IRS-1 and NEMO and mediates Ser^{307} phosphorylation of IRS-1. Furthermore, a low dose of insulin and an intact actin cytoskeleton may be necessary for clustering molecules related to TNF-α to down-regulate IRS-1.

Effects of NEMO and Myo1c expression on insulin signaling and glucose transport

Because IRS-1 protein is a key mediator of insulin signaling, we next focused on the roles of Myo1c and NEMO in insulin signaling and glucose transport. We prepared WT NEMO and NH_2-terminal–deleted (ΔN; residues 101–412) NEMO constructs

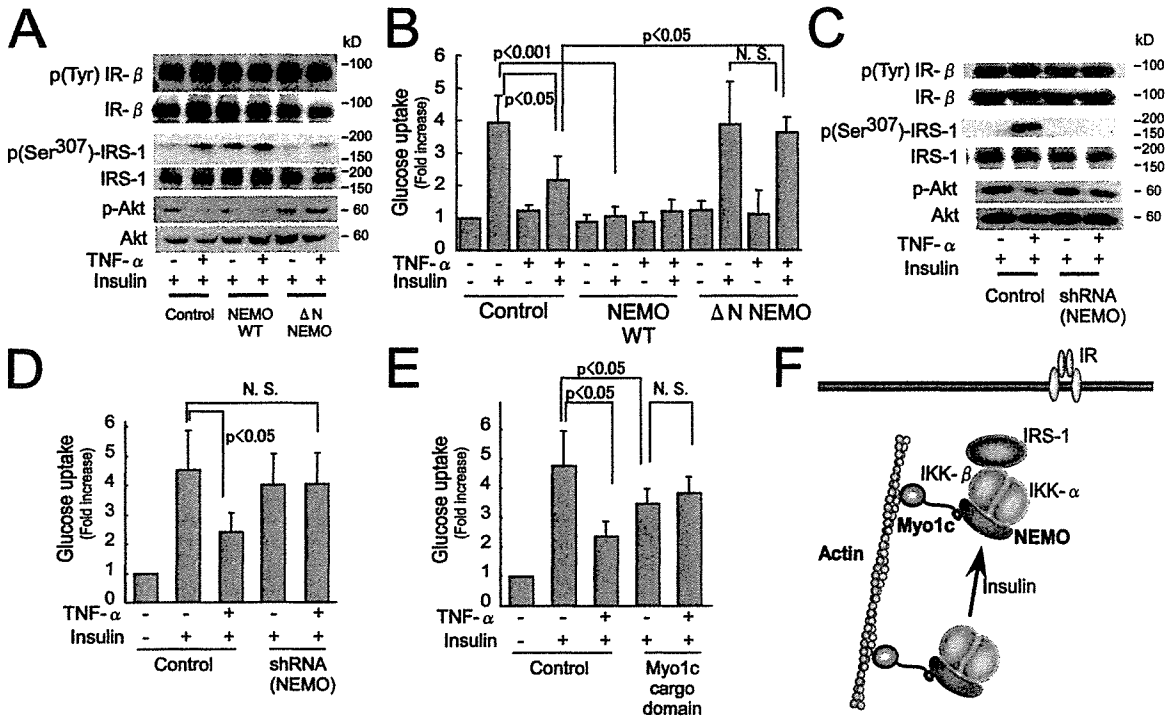

Figure 5. **NEMO and Myo1c for insulin signaling and glucose uptake in 3T3-L1 adipocytes.** (A–E) 3T3-L1 adipocytes were infected with recombinant adenovirus encoding wild type (WT) NEMO, ΔN-NEMO, shRNA (NEMO), Myo1c WT, Myo1c cargo domain, and vector alone (for control) at an MOI of 50. (A and C) The cells were serum starved for 2 h, treated with or without 20 ng/ml TNF-α for 15 min, and stimulated with or without 100 nM insulin for 10 min at 37°C. The cell lysates were immunoprecipitated with anti–insulin receptor β (IR-β) or anti–IRS-1 antibody, and the precipitates were immunoblotted with antiphosphotyrosine, anti–IR-β, anti–IRS-1, antiphospho-Ser^{307} IRS-1, antiphospho-Ser^{473} Akt, and anti-Akt antibodies. (B, D, and E) The cells were serum starved for 2 h in Krebs-Ringer phosphate buffer and treated with 20 ng/ml TNF-α for 4 h. Glucose uptake was measured. Each bar represents the mean ± SD (error bars) value of at least three independent experiments. (F) Schematic model of Myo1c-mediated IRS-1–IKK complex formation.

and performed a series of experiments. The NH_2 terminal of NEMO is the IKK-β–binding site, and deletion of this site was shown to impair the binding of NEMO with IKK-β (Yamamoto et al., 2001).

First, we assessed the effects of NEMO expression on upstream insulin signal cascades in 3T3-L1 adipocytes. Overexpression of WT NEMO induced the phosphorylation of IRS-1 Ser^{307} while decreasing Akt phosphorylation in the absence of TNF-α. Overexpression of ΔN-NEMO prevented the phosphorylation of IRS-1 Ser^{307} and inhibited Akt phosphorylation. We detected no changes in the tyrosine phosphorylation of the IR β chain (Fig. 5 A). Second, we measured 2-deoxyglucose uptake in 3T3-L1 adipocytes expressing NEMO constructs. Overexpression of WT NEMO abolished insulin-stimulated glucose uptake in the absence of TNF-α. In contrast, the overexpression of ΔN-NEMO completely blocked the inhibitory effects of TNF-α (Fig. 5 B). Third, we introduced shRNA into culture adipocytes to induce specific degradation of NEMO mRNA. NEMO protein expression was decreased to 20–30% of the control level (unpublished data). As expected, the deletion of NEMO almost completely blocked the inhibition of insulin-stimulated glucose uptake by TNF-α (Fig. 5 D). Under these conditions, IR-β tyrosine, IRS-1 Ser^{307}, and Akt Ser^{473} phosphorylations were examined in 3T3-L1 adipocytes. NEMO silencing by shRNA also prevented TNF-α–mediated IRS-1 Ser^{307} phosphorylation and inhibition of Akt phosphorylation without affecting IR tyrosine phosphorylation (Fig. 5 C). These data, combined with the data presented in Figs. 3 and 4, suggest that motor protein Myo1c and its receptor protein NEMO mediate TNF-α–induced down-regulation of IRS-1 and glucose uptake.

However, it was previously shown that the overexpression of ΔN-NEMO results in the loss of IKK kinase activity (Yamamoto et al., 2001). We confirmed the inhibition of IKK kinase activity in 3T3-L1 adipocytes expressing ΔN-NEMO as well as NEMO knockdown cells (Fig. S3, B and C). These observations indicated that NEMO plays a role in assembling the IKK complex and that this step is critical for IKK kinase activity. To avoid this bias and clarify the roles of Myo1c and NEMO in glucose uptake, we conducted another experiment using Myo1c cargo domain constructs. As shown in Fig. 5 E, overexpression of the cargo domain inhibited the TNF-α–induced suppression of glucose uptake. Together, these results provide evidence that NEMO may function as a receptor molecule for Myo1c and that Myo1c promotes the TNF-α–induced suppression of metabolic insulin action. In agreement with a previous study (Bose et al., 2002), we confirmed that Myo1c cargo domain expression itself decreased insulin-stimulated glucose uptake by 30%. This may be a result of the inhibitory role of Myo1c on GLUT4 recycling (Bose et al., 2002).

Based on the aforementioned data, we propose a simple model whereby Myo1c and its receptor NEMO cooperatively facilitate IKK–IRS-1 complex formation, as illustrated in Fig. 5 F. NEMO is a scaffold protein of the IKK complex. Recent studies suggest that some scaffold proteins serve as links between

molecular motors and intracellular vesicles, thereby functioning as cargo proteins (Dorner et al., 1999; Setou et al., 2000). In contrast, our data suggest that the scaffold protein NEMO links motor and signaling molecules as cargos. It is noteworthy that Myo1c organizes the signaling complex and serves as a platform for the two distinct signals to interact (i.e., the insulin signal and the TNF-α signal mediating insulin resistance).

Finally, our results allow us to draw three conclusions. First, the motor protein Myo1c appears to participate directly in the mechanism of IRS-1–IKK complex formation in culture adipocytes. It is possible that NEMO is a molecular receptor linking motor (Myo1c) and cargo (IKK-α and -β). Second, NEMO and Myo1c may be involved in the TNF-α–induced Ser^{307} phosphorylation of IRS-1, resulting in the attenuation of insulin signaling and glucose transport. Third, Myo1c and the actin cytoskeleton may facilitate formation of the signaling molecule complex that participates in the TNF-α–induced down-regulation of IRS-1. In summary, our data suggest that Myo1c and NEMO are responsible for the mechanism of TNF-α–induced insulin resistance.

Materials and methods

Constructs

Mouse full-length NEMO and IRS-1 were cloned by RT-PCR amplification with total mRNA from 3T3-L1 adipocytes. WT and an NH_2-terminal deletion mutant of NEMO containing amino acid residues 101–412 were subcloned into pEGFP-C2, pcDNA3.1His, pET-16b, and/or pGEX-6p-1 vectors. Mouse Myo1c cDNA was purchased from DNAFORM and subcloned into p3xFLAG-CMV7.1, pET-16b, and pGEX-6p-1 vectors. IKK-α and IKK-β cDNA were gifts from H. Nakano (Juntendo University School of Medicine, Tokyo, Japan).

Reagents and antibodies

The following antibodies were used: anti-NEMO, antiphospho-Ser^{307} IRS-1, and antiphospho-Akt antibodies (Cell Signaling); anti-NEMO and anti–IRS-1 antibodies (Upstate Biotechnology); anti-Flag antibody (Sigma-Aldrich); anti-Xpress antibody (Invitrogen); and Cy3-conjugated anti–mouse IgG (Jackson ImmunoResearch Laboratories). Rabbit polyclonal anti-Myo1c antibody was generated against the peptide sequence DKSELSDKKRPE. All other antibodies were purchased from Santa Cruz Biotechnology, Inc. AlexaFluor596-phalloidin was obtained from Invitrogen. Mouse TNF-α was purchased from PeproTech.

Cell culture

3T3-L1 fibroblasts were grown in DME with 10% FBS at 37°C. The cells (3–4-d after confluence) differentiated into adipocytes with incubation in the same DME containing 0.5 mM isobutylmethylxanthine, 0.25 μM dexamethasone, and 4 μg/ml insulin for 3 d and were then grown in DME with 10% FBS for an additional 3–6 d.

Immunofluorescence microscopy and digital image analysis

Differentiated 3T3-L1 adipocytes were transfected by electroporation. The cells were then replated onto coverslips and allowed to recover for 48 h followed by stimulation with 100 nM insulin or 20 ng/ml TNF-α for 15 min at 37°C. Then, 5 μM latrunculin B or 30 μM nocodazole were added 60 min before treatment with insulin. Minimum concentrations of these agents required for disrupting the cytoskeleton in culture adipocytes were determined previously (Emoto et al., 2001). Cells were fixed with 3.7% formaldehyde in PBS, permeabilized with buffer A (0.5% Triton X-100 and 1% FBS in PBS) for 15 min, and incubated for 2 h with primary antibodies at room temperature. The cells were washed and incubated with an appropriate secondary antibody or AlexaFluor596-phalloidin for 30 min. The coverslips were washed thoroughly and mounted on glass slides. Immunostained cells were observed at room temperature with a laser-scanning confocal microscope (LSM5 PASCAL; Carl Zeiss MicroImaging, Inc.) and its two-channel scanning module equipped with an inverted microscope (Axiovert 200M; Carl Zeiss MicroImaging, Inc.). The inverted microscope used the 63× NA 1.4 oil objective lens run by LSM5 processing software (Carl Zeiss MicroImaging, Inc.) and Adobe Photoshop CS2.

Preparation of adenovirus

Adenovirus producing mouse WT NEMO, deletion mutant NEMO (residues 101–412), mouse WT Myo1c, and dominant inhibitory Myo1c (residues 767–1,028) were prepared using an AdEasy Adenoviral Vetor System (Stratagene).

shRNA-induced degradation of NEMO

shRNA was designed to have a 5′-AAGGATTCGAGCAGTTAGTGAGC-3′ sequence. Synthetic complementary single-stranded oligonucleotide DNA was annealed, and the double-stranded DNA of the target sequence was created. This annealed DNA was inserted into a pcPUR+U6i cassette (Miyagishi and Taira, 2002), and the insert was transferred to an AdEasy Adenoviral Vector System. This shRNA system decreased NEMO protein expression to 20–30% of the control level.

Identification of NEMO-binding proteins

Myc-NEMO was expressed in 3T3-L1 adipocytes. 2 d thereafter, cells were serum starved for 2 h and stimulated with 100 nM insulin or 20 ng/ml TNF-α for 20 min. Cell lysates were prepared and immunoprecipitated with anti-myc antibody. Samples were resolved by SDS-PAGE, and proteins were visualized by silver staining. The bands were excised and subjected to in-gel digestion according to the method described by Shevchenko et al. (1996) with minor modifications. Mass spectra were acquired using a time of flight mass spectrometer (Voyager DE Pro; Applied Biosystems). The search engine for the peptide mass fingerprint was the web-based Mascot (Matrix Science).

Details of in-gel digestion. In brief, the gel pieces were washed twice in 300 μl CH_3CN for 30 min and dried. The gel pieces were then rehydrated in 100 μl of reduction buffer (10 mM DTT and 100 mM NH_4HCO_3) and were left standing at 56°C for 1 h. After supernatant removal, the gel pieces were incubated in 100 μl of 50 mM idotoacetamide in 100 mM NH_4HCO_3 for 45 min at room temperature. The gel pieces were then washed in 100 μl of 100 mM NH_4HCO_3 and dehydrated in 300 μl of acetonitrile. After washing and dehydration (twice each), the dried gel pieces were rehydrated on ice in 100 μl of digestion buffer (50 mM NH_4HCO_3 and 12.5 ng/μL each of lysylendopeptidase [Wako] and sequencing grade trypsin [Promega]) for 45 min. The supernatant was replaced with 50 mM NH_4HCO_3, and the gel pieces were incubated at 37°C overnight. The supernatant was collected, and the peptides were extracted repeatedly with a 50-μl solution of 5% (vol/vol) formic acid and 50% (vol/vol) acetonitrile by vortexing. The combined supernatants were evaporated to dryness in a vacuum centrifuge. Resulting peptides were redissolved in 0.1% trifluoroacetic acid and absorbed onto ZipTip C18 (Millipore). Bound peptides were eluted with 50% acetonitrile and 0.1% trifluoroacetic acid. Equal amounts of the resulting peptide solution and a matrix-assisted laser desorption ionization sample matrix solution (10 mg/ml α-cyano-4-hydroxycinnamic acid dissolved in 50% acetonitrile and 0.1% trifluoroacetic acid) were mixed on the sample target.

Pull-down assay

GST-fused NEMO and Myo1c were expressed using a pGEX-6p-1 vector in BL21 cells. His-tagged NEMO and Myo1c were expressed using a pET-16b vector in BL21 (DE3) cells. GST-fused protein and His-tagged protein were mixed in PBS and pulled down with glutathione–Sepharose beads (GE Healthcare). Protein interactions were detected by Western blotting using anti-His antibody and anti-GST antibody.

shRNA-induced degradation of Myo1c

Target sequences used in shRNA were the same as those described previously (Bose et al., 2002). Synthetic complementary single-stranded oligonucleotide DNAs were annealed to make double-stranded DNAs of the target sequences. These annealed DNA were inserted into a pcPUR+U6i cassette vector, and the plasmids were electroporated into differentiated 3T3-L1 adipocytes.

Immunoprecipitation and immunoblotting

Cells were lysed in lysis buffer (20 mM Hepes, pH 7.2, 100 mM NaCl, 1 mM EDTA, 25 mM NaF, 1 mM sodium vanadate, 1 mM benzamidine, 5 μg/ml leupeptin, 5 μg/ml aprotinin, 1 mM PMSF, and 1 mM DTT), and the protein concentration was measured with bicinchoninic acid protein assay reagent (Pierce Chemical Co.). For immunoprecipitation, the cell lysate was preincubated with protein G–Sepharose beads at 4°C for 30 min

to remove nonspecific bound protein. Then, samples were incubated with primary antibody at 4°C for 2 h followed by incubation with protein G–Sepharose beads. Lysates and immunoprecipitates were resolved by SDS-PAGE and transferred to a polyvinylidene difluoride membrane (GE Healthcare). The membrane was preblotted in milk buffer for 1 h and immunoblotted with primary antibody for 2 h. HRP-conjugated secondary antibodies (Jackson ImmunoResearch Laboratories) were used, and proteins were visualized using an enhanced chemiluminescence substrate kit (GE Healthcare).

2-deoxyglucose uptake

Differentiated adipocytes were prepared in 24-well plates. Cells were infected with the recombinant adenoviruses. 2 d thereafter, the cells were serum starved for 2 h at 37°C in Krebs-Ringer phosphate buffer (130 mM NaCl, 5 mM KCl, 1.3 mM $CaCl_2$, 1.3 mM $MgSO_4$, and 10 mM Na_2HPO_4, pH 7.4) and were treated with or without 20 ng/ml TNF-α for 4 h. Next, the cells were stimulated with or without 100 nM insulin for 5 min, and 2-deoxyglucose uptake was determined by 2-deoxy-D-[2,6 ^{3}H] glucose incorporation. Nonspecific deoxyglucose uptake was measured in the presence of 20 μM cytochalasin B and subtracted from each determination to obtain specific uptake. The deoxyglucose uptake was corrected using the protein amount.

In vitro kinase assay

3T3-L1 adipocytes were infected with the recombinant adenoviruses as indicated. 2 d after the infection, cells were stimulated with or without 20 ng/ml TNF-α for 5 min, and cell lysates were prepared. After adjusting the protein concentration, immunoprecipitation using anti–IKK-β antibody was performed. Precipitates were mixed with IKK substrate peptide (KKKKERLLDDRHDSGLDSMKDEE; Upstate Biotechnology) and γ-[^{32}P] ATP. After a 10-min incubation at 30°C, samples were transferred to P81 paper (Whatman) and washed with 0.75% phosphoric acid and acetone. Radioactivity was counted using a scintillation counter.

Statistical analysis

Multiple comparisons among groups were performed using the one-factor analysis of variance test (post-hoc test; Turkey-Kramer). Results are presented as means ± SD. Values of $P < 0.05$ were considered statistically significant.

Online supplemental material

Fig. S1 shows the results of pull-down experiments to demonstrate the direct interaction of NEMO with Myo1c. Fig. S2 shows the effects of NEMO knockdown on Myo1c–IKK-β interaction (A) and the effects of NEMO expression on IRS-1–IKK-β interaction (B). Fig. S3 shows the effects of Myo1c expression on the TNF-α–induced phosphorylation of IRS-1 Ser^{307} (A) and the effects of WT NEMO and ΔN-NEMO expression or NEMO knockdown on IKK-β kinase activity (B and C). Online supplemental material is available at http://www.jcb.org/cgi/content/full/jcb.200601065/DC1.

We thank Dr. Hiroyasu Nakano for providing the IKK-α and -β constructs. We are also grateful to Dr. Teruo Nishida (Yamaguchi University Graduate School of Medicine, Yamaguchi, Japan) for allowing us to use his confocal microscope.

This work was partly supported by Grants-in-Aid for Scientific Research (KAKENHI) from the Ministry of Education, Culture, Sports, Science and Technology of Japan (15590940 and 17590934) to M. Emoto and the Research Grant for Longevity Sciences from the Ministry of Health, Labor, and Welfare of Japan (15C-8) to Y. Tanizawa.

Submitted: 12 January 2006
Accepted: 1 May 2006

References

Bose, A., A. Guilherme, S.I. Robida, S.M. Nicoloro, Q.L. Zhou, Z.Y. Jiang, D.P. Pomerleau, and M.P. Czech. 2002. Glucose transporter recycling in response to insulin is facilitated by myosin Myo1c. *Nature*. 420:821–824.

de Alvaro, C., T. Teruel, R. Hernandez, and M. Lorenzo. 2004. Tumor necrosis factor α produces insulin resistance in skeletal muscle by activation of inhibitor κB kinase in a p38 MAPK-dependent manner. *J. Biol. Chem.* 279:17070–17078.

DiDonato, J.A., M. Hayakawa, D.M. Rothwarf, E. Zandi, and M. Karin. 1997. A cytokine-responsive IκB kinase that activates the transcription factor NF-κB. *Nature*. 388:548–554.

Dorner, C., A. Ullrich, H.U. Haring, and R. Lammers. 1999. The kinesin-like motor protein KIF1C occurs in intact cells as a dimer and associates with proteins of the 14-3-3 family. *J. Biol. Chem.* 274:33654–33660.

Emoto, M., S.E. Langille, and M.P. Czech. 2001. A role for kinesin in insulin-stimulated GLUT4 glucose transporter translocation in 3T3-L1 adipocytes. *J. Biol. Chem.* 276:10677–10682.

Gao, Z., D. Hwang, F. Bataille, M. Lefevre, D. York, M.J. Quon, and J. Ye. 2002. Serine phosphorylation of insulin receptor substrate 1 by inhibitor κB kinase complex. *J. Biol. Chem.* 277:48115–48121.

Hotamisligil, G.S., N.S. Shargill, and B.M. Spiegelman. 1993. Adipose expression of tumor necrosis factor-α: direct role in obesity-linked insulin resistance. *Science*. 259:87–91.

Kanety, H., R. Feinstein, M.Z. Papa, R. Hemi, and A. Karasik. 1995. Tumor necrosis factor α-induced phosphorylation of insulin receptor substrate-1 (IRS-1). Possible mechanism for suppression of insulin-stimulated tyrosine phosphorylation of IRS-1. *J. Biol. Chem.* 270:23780–23784.

Kim, J.K., Y.J. Kim, J.J. Fillmore, Y. Chen, I. Moore, J. Lee, M. Yuan, Z.W. Li, M. Karin, P. Perret, et al. 2001. Prevention of fat-induced insulin resistance by salicylate. *J. Clin. Invest.* 108:437–446.

Luo, J., S.J. Field, J.Y. Lee, J.A. Engelman, and L.C. Cantley. 2005. The p85 regulatory subunit of phosphoinositide 3-kinase down-regulates IRS-1 signaling via the formation of a sequestration complex. *J. Cell Biol.* 170:455–464.

Miyagishi, M., and K. Taira. 2002. U6 promoter-driven siRNAs with four uridine 3′ overhangs efficiently suppress targeted gene expression in mammalian cells. *Nat. Biotechnol.* 20:497–500.

Nakano, H., M. Shindo, S. Sakon, S. Nishinaka, M. Mihara, H. Yagita, and K. Okumura. 1998. Differential regulation of IκB kinase α and β by two upstream kinases, NF-κB–inducing kinase and mitogen-activated protein kinase/ERK kinase kinase-1. *Proc. Natl. Acad. Sci. USA*. 95:3537–3542.

Reaven, G.M. 1988. Banting lecture 1988. Role of insulin resistance in human disease. *Diabetes*. 37:1595–1607.

Setou, M., T. Nakagawa, D.H. Seog, and N. Hirokawa. 2000. Kinesin superfamily motor protein KIF17 and mLin-10 in NMDA receptor-containing vesicle transport. *Science*. 288:1796–1802.

Shevchenko, A., M. Wilm, O. Vorm, and M. Mann. 1996. Mass spectrometric sequencing of proteins from silver-stained polyacrylamide gels. *Anal. Chem.* 68:850–858.

Weil, R., K. Schwamborn, A. Alcover, C. Bessia, V. Di Bartolo, and A. Israel. 2003. Induction of the NF-κB cascade by recruitment of the scaffold molecule NEMO to the T cell receptor. *Immunity*. 18:13–26.

Williamson, R.T., and M.D. Lond. 1901. On the treatment of glycosuria and diabetes mellitus with sodium salicylate. *Brit. Med. J.* 1:760–762.

Yamamoto, Y., D.W. Kim, Y.T. Kwak, S. Prajapati, U. Verma, and R.B. Gaynor. 2001. IKKγ /NEMO facilitates the recruitment of the IκB proteins into the IκB kinase complex. *J. Biol. Chem.* 276:36327–36336.

Yamaoka, S., G. Courtois, C. Bessia, S.T. Whiteside, R. Weil, F. Agou, H.E. Kirk, R.J. Kay, and A. Israel. 1998. Complementation cloning of NEMO, a component of the IκB kinase complex essential for NF-κB activation. *Cell*. 93:1231–1240.

Yin, M.J., Y. Yamamoto, and R.B. Gaynor. 1998. The anti-inflammatory agents aspirin and salicylate inhibit the activity of IκB kinase-β. *Nature*. 396:77–80.

Yuan, M., N. Konstantopoulos, J. Lee, L. Hansen, Z.W. Li, M. Karin, and S.E. Shoelson. 2001. Reversal of obesity- and diet-induced insulin resistance with salicylates or targeted disruption of Ikkβ. *Science*. 293:1673–1677.

Available online at www.sciencedirect.com
SCIENCE DIRECT
DIABETES RESEARCH AND CLINICAL PRACTICE
ELSEVIER
Diabetes Research and Clinical Practice 73 (2006) 215–217
www.elsevier.com/locate/diabres

Brief report

A novel mutation of *WFS1* gene in a Japanese man of Wolfram syndrome with positive diabetes-related antibodies

Akinobu Nakamura [a], Chikara Shimizu [a,*], So Nagai [a], Satoshi Taniguchi [a], Masaaki Umetsu [a], Toshiya Atsumi [a], Norio Wada [a], Narihito Yoshioka [a], Yuri Ono [a], Yukio Tanizawa [b], Takao Koike [a]

[a] *Department of Medicine II, Hokkaido University Graduate School of Medicine, N-15, W-7, Kita-ku, Sapporo 060-8638, Japan*
[b] *Division of Molecular Analysis of Human Disorders, Department of Bio-Signal Analysis, Yamaguchi University Graduate School of Medicine, Minamikogushi 1-1-1, Ube 755-8505, Japan*

Received 28 October 2005; accepted 23 December 2005
Available online 25 January 2006

Abstract

Wolfram syndrome is a rare, autosomal recessive disorder characterized by early-onset diabetes mellitus, optic atrophy and neurological and endocrinological abnormalities. A 47-year-old Japanese man with frequent severe hypoglycemic episodes was diagnosed as Wolfram syndrome based on clinical features and laboratory data. He had positive glutamic acid decarboxylase (GAD) and insulinoma-associated antigen-2 (IA-2) antibodies, both uncommon in this syndrome. Genetic analysis revealed that *WFS1* gene of the patient has a homozygous 5 base pairs (AAGGC) insertion at position 1279 in exon 8, causing a frameshift at codon 371 leading to premature termination at codon 443.

Keywords: Wolfram syndrome; GAD antibody; IA-2 antibody; *WFS1* gene

Wolfram syndrome (WS), also referred to as DIDMOAD syndrome, is an autosomal recessively inherited syndrome first described by Wolfram and Wagener [1]. It is a progressive neurodegenerative syndrome characterized by diabetes insipidus, diabetes mellitus, optic atrophy and deafness. WS is rare with an estimated general prevalence of 1:770,000 and a carrier frequency of 1:354 [2]. In 1998, a nuclear gene responsible for WS, *WFS1*, was identified and mapped to chromosome 4p16.1 using positional cloning [3].

The following report is of a patient diagnosed with WS having positive glutamic acid decarboxylase (GAD) and insulinoma-associated antigen-2 (IA-2) antibodies. The diabetogenic mechanism in this syndrome has apparently not been recognized as an autoimmune process. Furthermore, we identified a novel mutation in the *WFS1* gene of the patient.

A 47-year-old Japanese man was admitted to our hospital because of frequent severe hypoglycemic episodes. Diabetes was diagnosed and insulin treatment was started when he was 6 years. Progressive loss of vision was observed at the age of 11 and hearing loss at 19 years. At the age of 24 years, he was aware of difficulty in urinating, which required daily bladder catheterizations. His parents, who are healthy as is the older brother, are consanguineous. No hereditary disease in the ascendants was found.

On physical examination, height was 165.1 cm and weight was 37.3 kg. Blood pressure was 108/62 mmHg,

* Corresponding author. Tel.: +81 11 706 5915; fax: +81 11 706 7710.
E-mail address: shimizch@med.hokudai.ac.jp (C. Shimizu).

0168-8227/$ – see front matter © 2006 Elsevier Ireland Ltd. All rights reserved.
doi:10.1016/j.diabres.2005.12.007

Table 1
Diabetes-related findings

Fasting plasma glucose (mg/dl)	109
Glycohemoglobin A_{1c} (HbA_{1c}) (%)	9.2
Urinary output of C peptide reactivity (CPR) (μg/day)	<0.7
Plasma CPR to glucagon (0–6 min) (ng/ml)	<0.05 to <0.05
Urinary microalbumin (mg/day)	3.2
Glutamic acid decarboxylase (GAD) antibody	(+)
Insulinoma-associated antigen-2 (IA-2) antibody	(+)
Autoantibodies to iscet cells (ICA)	(−)
Human leucocyte antigen (HLA)	DR-4, DR-8
Mitochondrial tRNA Leu (3243) mutation	(−)

and pulse rate was regular at 66 min^{-1}. There were no remarkable findings in heart, lung and abdomen. Neurological abnormalities such as cerebellar ataxia and myoclonus were not found except for the absence of Achilles tendon reflex. Psychiatric disorders such as depression and psychosis were not found.

In general laboratory findings, urine sugar was detected. Other general biochemical markers including renal function, electrolytes and lipid profiles were within normal range as were serum concentrations of lactate and pyruvate.

Diabetes-related findings are shown in Table 1. Diabetic neuropathy was found, but diabetic nephropathy and diabetic retinopathy were not. A high level of glycohemoglobin A_{1c} (HbA_{1c}), an extremely low level of urinary output of C peptide reactivity (CPR) and unresponsiveness of CPR to glucagon loading test were comparable with insulin-dependent diabetes mellitus commonly seen in patients with WS. However, GAD and IA-2 antibodies were detected, being uncommon in WS. Autoantibodies to islet cells were negative. Human leucocyte antigen (HLA) typing of DR was DR-4 and DR-8. The mitochondrial tRNA Leu (3243) mutation was absent.

Optic atrophy was confirmed by fundascopy and a bilateral symmetric sensorineural hearing loss prevalent for the medium–high frequencies was demonstrated by audiometry. Urodynamics testings showed bladder atony regardless of no upper urinary tract abnormalities. Brain magnetic resonance imaging (MRI) showed the absence of posthypophysis signals, but other MRI abnormalities such as cerebellar and brain stem atrophy were not found. To confirm the presence of diabetes insipidus (DI), hypertonic saline test was done. Arginine vasopressin (AVP) was not responsive to 5% hypertonic saline infusion (from 1.48 pmol/l to 1.48 pmol/l), which confirmed the diagnosis of DI.

Genetic analysis was made under the approval of the institutional review board and written informed consent. Using genomic DNA extracted from peripheral blood mononuclear cells, all exons of *WFS1* gene were amplified by polymerase-chain-reaction (PCR) and directly sequenced, as described in a previous report [3]. The patient has a homozygous 5 base pairs (AAGGC) insertion at position 1279 in exon 8 which causes a frameshift at codon 371 leading to premature termination at codon 443. Family analysis demonstrated that his parents but not his brother are heterozygous for the same mutation as the patient. Family members other than the patient did not show any signs suggesting WS.

There are several clear distinctions between WS-associated diabetes and classic type 1 diabetes. It is well established that genes in the HLA region contribute to predisposition to typical type 1 diabetes. However, previous studies failed to find an influence of HLA on WS [4,5]. A second distinction is the apparent absence of an autoimmune process in WS-associated diabetes [6]. The lack of islet cell antibodies has been reported for most cases and GAD antibodies were negative in all studied, respectively [2,7].

The diabetes mellitus associated with WS is clearly related to loss of β cells in the pancreas [8,9]. In one series of an autopsy study, loss of β cells or atrophy of the islets was noted in 9 of 11 of WS patients [8]. The exocrine portion of the pancreas was reported to be normal with the exception of focal areas of fibrosis [9]. Immunohistochemical studies of the pancreas reveal normal staining for glucagon, somatostatin, and pancreatic polypeptide but the virtual absence of cells staining for insulin. This indicates a selective β cell loss with preservation of α and δ cells in the islets [9] and allows for the conclusion that diabetes in WS is caused not by a functional defect in the β cells, but by actual β cell depletion.

In our case, HLA typing of DR was DR-4 and DR-8 which is an increased risk for Japanese juvenile-onset type 1 diabetes [10]. In addition, serological examination showed positive GAD and IA-2 antibodies. These results suggest that the diabetes in our patient was caused by an immune-mediated destruction of the insulin-producing β cells of the pancreas in addition to a selective β cell loss not been described previously in this syndrome.

Many mutations, along the entire gene, with homozygous and compound heterozygous mutations, have been described since the identification of *WFS1* as the cause of WS. The patient had a novel homozygous

insertion mutation causing a frameshift at codon 371 leading to premature termination at codon 443, resulting in a complete absence of the carboxy tail of the *WFS1* protein. Although function of *WFS1* gene has not been fully elucidated, a role in membrane trafficking, protein processing, or calcium homeostasis in the endoplasmic reticulum has been postulated [11].

Furthermore, it is speculated that the carboxy tail is interacting with other, unknown proteins [11]. Expression studies of mutant proteins are necessary to determine which parts of the protein are essential for biological function.

In summary, we have reported a case of WS patient carrying a novel mutation in *WFS1* gene with positive GAD and IA-2 antibodies. In the present case, the diabetes might be caused by an immune-mediated destruction and a selective loss of the insulin-producing β cells of the pancreas. In addition, further molecular analysis is necessary to uncover the pathogenesis of this syndrome.

References

[1] D.J. Wolfram, H. Wagener, Diabetes mellitus and simple optic atrophy among siblings: report of four cases, Mayo Clin. Proc. 9 (1938) 715–718.

[2] T.G. Barrett, S.E. Bundey, A.F. Macleod, Neurodegeneration and diabetes: U.K. nationwide study of Wolfram (DIDMOAD) syndrome, Lancet 346 (1995) 1458–1463.

[3] H. Inoue, Y. Tanizawa, J. Wasson, P. Behn, K. Kalidas, E. Bernal-Mizrachi, et al., A gene encoding a transmembrane protein is mutated in patients with diabetes mellitus and optic atrophy (Wolfram syndrome), Nat. Genet. 20 (1998) 143–148.

[4] B.T. Kinsley, R.G. Firth, The Wolfram syndrome: a primary neurodegenerative disorder with lethal potential, Ir. Med. J. 85 (1992) 34–36.

[5] C.A. Stanley, R.S. Spielman, C.M. Zmijewski, L. Baker, Wolfram syndrome not HLA linked, N. Engl. J. Med. 301 (1979) 1398–1399.

[6] C. Blasi, F. Pierelli, E. Rispoli, M. Saponara, E. Vingolo, D. Andreani, Wolfram's syndrome: a clinical, diagnostic, and interpretative contribution, Diab. Care 9 (1986) 521–528.

[7] R. Medlej, J. Wasson, P. Baz, S. Azar, I. Salti, J. Loiselet, et al., Diabetes mellitus and optic atrophy: a study of Wolfram syndrome in the Lebanese population, J. Clin. Endocrinol. Metab. 89 (2004) 1656–1661.

[8] B.T. Kinsley, R.H. Dumont, M. Swift, R.G. Swift, Morbidity and mortality in the Wolfram syndrome, Diab. Care 18 (1995) 1566–1570.

[9] A. Karasik, C. O'Hara, S. Srikanta, M. Swift, J.S. Soeldner, C.R. Kahn, et al., Genetically programmed selective islet beta-cell loss in diabetic subjects with Wolfram's syndrome, Diab. Care 12 (1989) 135–138.

[10] S. Murao, H. Makino, Y. Kaino, E. Konoue, J. Ohashi, K. Kida, et al., Differences in the contribution of HLA-DR and -DQ haplotypes to susceptibility to adult- and childhood-onset type 1 diabetes in Japanese patients, Diabetes 53 (2004) 2684–2690.

[11] J.M. van ven Ouweland, K. Cryns, R.J. Pennings, I. Walraven, G.M. Janssen, J.A. Maassen, et al., Molecular characterization of WFS1 in patients with Wolfram syndrome, J. Mol. Diagn. 5 (2003) 88–95.

Brief Genetics Report

Association Studies of Variants in the Genes Involved in Pancreatic β-Cell Function in Type 2 Diabetes in Japanese Subjects

Norihide Yokoi,[1] Masao Kanamori,[2] Yukio Horikawa,[3] Jun Takeda,[3] Tokio Sanke,[4] Hiroto Furuta,[5] Kishio Nanjo,[5] Hiroyuki Mori,[6] Masato Kasuga,[6] Kazuo Hara,[7] Takashi Kadowaki,[7] Yukio Tanizawa,[8] Yoshitomo Oka,[9] Yukiko Iwami,[10] Hisako Ohgawara,[10] Yuichiro Yamada,[11] Yutaka Seino,[11] Hideki Yano,[12] Nancy J. Cox,[13] and Susumu Seino[1]

Because impaired insulin secretion is characteristic of type 2 diabetes in Asians, including Japanese, the genes involved in pancreatic β-cell function are candidate susceptibility genes for type 2 diabetes. We examined the association of variants in genes encoding several transcription factors (*TCF1*, *TCF2*, *HNF4A*, *ISL1*, *IPF1*, *NEUROG3*, *PAX6*, *NKX2–2*, *NKX6–1*, and *NEUROD1*) and genes encoding the ATP-sensitive K^+ channel subunits Kir6.2 (*KCNJ11*) and SUR1 (*ABCC8*) with type 2 diabetes in a Japanese cohort of 2,834 subjects. The exon 16 −3c/t variant rs1799854 in *ABCC8* showed a significant association ($P = 0.0073$), and variants in several genes showed nominally significant associations ($P < 0.05$) with type 2 diabetes. Although the E23K variant rs5219 in *KCNJ11* showed no association with diabetes in Japanese (for the K allele, odds ratio [OR] 1.08 [95% CI 0.97–1.21], $P = 0.15$), 95% CI around the OR overlaps in meta-analysis of European populations, suggesting that our results are not inconsistent with the previous studies. This is the largest association study so far conducted on these genes in Japanese and provides valuable information for comparison with other ethnic groups. *Diabetes* 55:2379–2386, 2006

From the [1]Division of Cellular and Molecular Medicine, Kobe University Graduate School of Medicine, Kobe, Japan; the [2]Division of Health and Preventive Medicine, Department of Lifelong Sport, Biwako Seikei Sport College, Shiga, Japan; the [3]Department of Endocrinology, Diabetes and Rheumatology, Division of Bioregulatory Medicine, Gifu University School of Medicine, Gifu, Japan; the [4]Department of Clinical Laboratory Medicine, Wakayama University of Medical Science, Wakayama, Japan; the [5]First Department of Medicine, Wakayama University of Medical Science, Wakayama, Japan; the [6]Department of Clinical Molecular Medicine, Division of Diabetes and Digestive and Kidney Diseases, Kobe University Graduate School of Medicine, Kobe, Japan; the [7]Department of Metabolic Diseases, Graduate School of Medicine, University of Tokyo, Tokyo, Japan; the [8]Division of Molecular Analysis of Human Disorders, Department of Bio-Signal Analysis, Yamaguchi University Graduate School of Medicine, Ube, Japan; the [9]Division of Molecular Metabolism and Diabetes, Tohoku University Graduate School of Medicine, Sendai, Japan; the [10]Division of Cell Replacement and Regenerative Medicine, Medical Research Institute, School of Medicine, Tokyo Women's Medical University, Tokyo, Japan; the [11]Department of Diabetes and Clinical Nutrition, Kyoto University Graduate School of Medicine, Kyoto, Japan; the [12]Department of Internal Medicine, Hikone Municipal Hospital, Shiga, Japan; and the [13]Departments of Medicine and Human Genetics, University of Chicago, Chicago, Illinois.

Address correspondence and reprint requests to Susumu Seino, Division of Cellular and Molecular Medicine, Kobe University Graduate School of Medicine, Chuo-ku, Kobe 650-0017, Japan. E-mail: seino@med.kobe-u.ac.jp.

Received for publication 13 September 2005 and accepted in revised form 22 May 2006.

Additional information for this article can be found in an online appendix at http://diabetes.diabetesjournals.org.

HWE, Hardy-Weinberg equilibrium; K_{ATP} channel, ATP-sensitive K^+ channel; LD, linkage disequilibrium; SNP, single nucleotide polymorphism.

DOI: 10.2337/db05-1203

Impaired insulin secretion and insulin resistance both contribute to the pathogenesis of type 2 diabetes. The former is a characteristic feature of type 2 diabetes, especially in Asians including Japanese (1), and genes encoding proteins critical in pancreatic β-cell function are therefore particularly good candidate susceptibility genes for type 2 diabetes for this population. Studies of maturity-onset diabetes of the young in humans (2) and knockout mice (3) have shown that mutations of transcription factors required for development, differentiation, and maintenance of the pancreatic β-cells can cause diabetes. Pancreatic β-cell ATP-sensitive K^+ channels (K_{ATP} channels) are crucial in the regulation of insulin secretion by coupling cell metabolism to membrane electrical activity. The pancreatic β-cell K_{ATP} channel comprises two subunits, the inwardly rectifying potassium channel Kir6.2 (*KCNJ11*) and the sulfonylurea receptor SUR1 (*ABCC8*) (4). Mutations in the genes (*ABCC8* and *KCNJ11*) can cause familial persistent hyperinsulinemic hypoglycemia of infancy (5) and permanent neonatal diabetes (6). Several polymorphisms in these genes also have been reported to be associated with type 2 diabetes in populations with distinct ethnic backgrounds (7–20). However, a large-scale association study of these genes has not been performed in type 2 diabetes in the Japanese population. Here, we report on the association of variants in genes encoding various transcription factors and pancreatic β-cell K_{ATP} channel subunits with type 2 diabetes in a large Japanese cohort.

A case-control association study using 1,590 Japanese diabetic subjects and 1,244 nondiabetic control subjects was performed. All subjects were genotyped for 33 variants of 12 genes including transcription factors (*TCF1*, *TCF2*, *HNF4A*, *ISL1*, *IPF1*, *NEUROG3*, *PAX6*, *NKX2–2*, *NKX6–1*, and *NEUROD1*) and β-cell K_{ATP} channel subunits (*KCNJ11* and *ABCC8*) (Table 1).

Results of Hardy-Weinberg equilibrium (HWE) tests are shown in Table 1 of the online appendix (available at http://diabetes.diabetesjournals.org). All genotypes were in HWE, except for departures in cases at *TCF2*_SNP (single nucleotide polymorphism) 5 rs2689, *TCF2*_SNP6

TABLE 1
Summary of association studies of 33 variants for 12 genes with type 2 diabetes

Number	Locus	HapMap data	Subject	Allele data (frequency) 1	Allele data (frequency) 3	Genotype data (frequency) 1	Genotype data (frequency) 2	Genotype data (frequency) 3	*P* value Allele 2*2	*P* value Genotype 2*3	OR (95% CI)
1	TCF1_SNP1			A	C	A/A	A/C	C/C			
	rs1169288	JPT	Case	1,590 (0.50)	1,590 (0.50)	385 (0.24)	820 (0.52)	385 (0.24)	0.4508	0.2388	1.04 (0.94–1.16)
	I27L		Control	1,270 (0.51)	1,218 (0.49)	332 (0.27)	606 (0.49)	306 (0.25)			
2	TCF1_SNP2			G	A	G/G	G/A	A/A			
	rs1169294	none	Case	1,702 (0.54)	1,478 (0.46)	443 (0.28)	816 (0.51)	331 (0.21)	0.3247	0.1566	1.06 (0.95–1.17)
	IVS1 −42		Control	1,298 (0.52)	1,190 (0.48)	348 (0.28)	602 (0.48)	294 (0.24)			
3	TCF1_SNP3			A	T	A/A	A/T	T/T			
	rs2071190	JPT	Case	482 (0.15)	2,698 (0.85)	38 (0.02)	406 (0.26)	1,146 (0.72)	0.8925	0.8617	1.01 (0.87–1.17)
	IVS2 −51		Control	373 (0.15)	2,115 (0.85)	26 (0.02)	321 (0.26)	897 (0.72)			
4	TCF2_SNP1			G	A	G/G	G/A	A/A			
	rs757210	JPT	Case	2,079 (0.65)	1,101 (0.35)	697 (0.44)	685 (0.43)	208 (0.13)	0.4565	0.2695	1.04 (0.93–1.17)
	IVS2 + 2916		Control	1,651 (0.66)	837 (0.34)	546 (0.44)	559 (0.45)	139 (0.11)			
5	TCF2_SNP2			A	G	A/A	A/G	G/G			
	rs757211	none	Case	1,460 (0.46)	1,720 (0.54)	342 (0.22)	776 (0.49)	472 (0.30)	0.6994	0.5473	1.02 (0.92–1.14)
	IVS2 + 2953		Control	1,156 (0.46)	1,332 (0.54)	262 (0.21)	632 (0.51)	350 (0.28)			
6	TCF2_SNP3			G	A	G/G	G/A	A/A			
	rs718960	JPT	Case	2,288 (0.72)	892 (0.28)	824 (0.52)	640 (0.40)	126 (0.08)	0.6121	0.8597	1.03 (0.92–1.16)
	IVS4 + 14307		Control	1,774 (0.71)	714 (0.29)	632 (0.51)	510 (0.41)	102 (0.08)			
7	TCF2_SNP4			T	A	T/T	T/A	A/A			
	rs1016991	JPT	Case	2,823 (0.89)	357 (0.11)	1,260 (0.79)	303 (0.19)	27 (0.02)	0.0105*	0.0399*	1.23 (1.05–1.45)
	IVS8 + 929		Control	2,152 (0.87)	336 (0.14)	938 (0.75)	276 (0.22)	30 (0.02)			
8	TCF2_SNP5			A	T	A/A	A/T	T/T			
	rs2689	JPT	Case	1,722 (0.54)	1,458 (0.46)	488 (0.31)	746 (0.47)	356 (0.22)	0.5195	0.3582	1.04 (0.93–1.15)
	+274 TGA		Control	1,325 (0.53)	1,163 (0.47)	355 (0.29)	615 (0.49)	274 (0.22)			
9	TCF2_SNP6			A	C	A/A	A/C	C/C			
	rs2688	JPT	Case	1,840 (0.58)	1,340 (0.42)	552 (0.35)	736 (0.46)	302 (0.19)	0.0563	0.0291*	1.11 (1.00–1.24)

	+444 TGA		Control	1,503 (0.60)	985 (0.40)	448 (0.36)	607 (0.49)	189 (0.15)			
10	HNF4A_SNP1			T	C	T/T	T/C	C/C			
	rs717247	JPT	Case	2,277 (0.72)	903 (0.28)	811 (0.51)	655 (0.41)	124 (0.08)	0.2071	0.4223	1.08 (0.96–1.22)
	−4229		Control	1,820 (0.73)	668 (0.27)	661 (0.53)	498 (0.40)	85 (0.07)			
11	HNF4A_SNP2			A	G	A/A	A/G	G/G			
	rs736820	none	Case	1,207 (0.38)	1,973 (0.62)	230 (0.14)	747 (0.47)	613 (0.39)	0.4482	0.6472	1.04 (0.94–1.16)
	IVS1 + 3889		Control	919 (0.37)	1,569 (0.63)	176 (0.14)	567 (0.46)	501 (0.40)			
12	HNF4A_SNP3			T	C	T/T	T/C	C/C			
	rs745975	JPT	Case	643 (0.20)	2,537 (0.80)	53 (0.03)	537 (0.34)	1,000 (0.63)	0.0470*	0.0769	1.15 (1.00–1.31)
	IVS1 −5		Control	450 (0.18)	2,038 (0.82)	39 (0.03)	372 (0.30)	833 (0.67)			
13	ISL1_SNP10			G	A	G/G	G/A	A/A			
	rs2303750	none	Case	2,842 (0.89)	338 (0.11)	1,271 (0.80)	300 (0.19)	19 (0.01)	0.5101	0.4453	1.06 (0.90–1.26)
	IVS3 −4		Control	2,209 (0.89)	279 (0.11)	987 (0.79)	235 (0.19)	22 (0.02)			
14	ISL1_SNP11			A	G	A/A	A/G	G/G			
	rs2303751	none	Case	2,466 (0.78)	714 (0.22)	958 (0.60)	550 (0.35)	82 (0.05)	0.0539	0.1224	1.14 (1.00–1.29)
	P165P		Control	1,983 (0.80)	505 (0.20)	787 (0.63)	409 (0.33)	48 (0.04)			
15	IPF1_SNP3			G	T	G/G	G/T	T/T			
	rs4430606	none	Case	1,688 (0.53)	1,492 (0.47)	451 (0.28)	786 (0.49)	353 (0.22)	0.1807	0.3405	1.06 (0.90–1.26)
	IVS1 + 512		Control	1,366 (0.55)	1,122 (0.45)	371 (0.30)	624 (0.50)	249 (0.20)			
16	IPF1_SNP4			A	C	A/A	A/C	C/C			
	rs1124607	JPT	Case	2,527 (0.79)	653 (0.21)	1,007 (0.63)	513 (0.32)	70 (0.04)	0.7609	0.6259	1.02 (0.90–1.16)
	IVS1 + 539		Control	1,968 (0.79)	520 (0.21)	788 (0.63)	392 (0.32)	64 (0.05)			
17	IPF1_SNP7			G	A	G/G	G/A	A/A			
	none	none	Case	2,836 (0.89)	344 (0.11)	1,260 (0.79)	316 (0.20)	14 (0.01)	0.1309	0.2318	1.14 (0.97–1.34)
	IVS1 + 1787		Control	2,186 (0.88)	302 (0.12)	953 (0.77)	280 (0.23)	11 (0.01)			

Continued on following page

TABLE 1
Continued

Number	Locus	HapMap data	Subject	Allele data (frequency) 1	Allele data (frequency) 3	Genotype data (frequency) 1	Genotype data (frequency) 2	Genotype data (frequency) 3	*P* value Allele 2*2	*P* value Genotype 2*3	OR (95% CI)
18	NEUROG3_SNP1			A	G	A/A	A/G	G/G			
	rs3812704	JPT	Case	1,472 (0.46)	1,708 (0.54)	337 (0.21)	798 (0.50)	455 (0.29)	0.2674	0.4687	1.06 (0.96–1.18)
	−1822		Control	1,114 (0.45)	1,374 (0.55)	252 (0.20)	610 (0.49)	382 (0.31)			
19	NEUROG3_SNP2			T	C	T/T	T/C	C/C			1.06 (0.95–1.19)
	rs4536103	JPT	Case	2,268 (0.71)	912 (0.29)	798 (0.50)	672 (0.42)	120 (0.08)	0.3129	0.2040	
	F199S		Control	1,743 (0.70)	745 (0.30)	616 (0.50)	511 (0.41)	117 (0.09)			
20	PAX6_SNP1			A	T	A/A	A/T	T/T			1.08 (0.97–1.20)
	rs2239789	none	Case	1,725 (0.54)	1,455 (0.46)	483 (0.30)	759 (0.48)	348 (0.22)	0.1697	0.2391	
	IVS6 + 282		Control	1,396 (0.56)	1,092 (0.44)	392 (0.32)	612 (0.49)	240 (0.19)			
21	PAX6_SNP2			C	T	C/C	C/T	T/T			1.01 (0.86–1.18)
	rs667773	none	Case	2,791 (0.88)	389 (0.12)	1,228 (0.77)	335 (0.21)	27 (0.02)	0.9358	0.8923	
	IVS7 + 218		Control	2,181 (0.88)	307 (0.12)	961 (0.77)	259 (0.21)	24 (0.02)			
22	NKX2-2_SNP1			T	C	T/T	T/C	C/C			1.08 (0.74–1.56)
	none	none	Case	3,117 (0.98)	63 (0.02)	1,530 (0.96)	57 (0.04)	3 (0.002)	0.7650	0.8727	
	+856 TGA		Control	2,435 (0.98)	53 (0.02)	1,193 (0.96)	49 (0.04)	2 (0.002)			
23	NKX2-2_SNP2			C	T	C/C	C/T	T/T			1.13 (1.02–1.25)
	rs3746741	none	Case	1,666 (0.52)	1,514 (0.48)	452 (0.28)	762 (0.48)	376 (0.24)	0.0251*	0.0563	
	+1163 TGA		Control	1,228 (0.49)	1,260 (0.51)	305 (0.25)	618 (0.50)	321 (0.26)			
24	NKX6-1_SNP1			A	C	A/A	A/C	C/C			1.03 (0.92–1.16)
	rs1017560	JPT	Case	2,182 (0.69)	998 (0.31)	747 (0.47)	688 (0.43)	155 (0.10)	0.6052	0.0144*	
	−15606		Control	1,724 (0.69)	764 (0.31)	625 (0.50)	474 (0.38)	145 (0.12)			
25	NKX6-1_SNP2			T	G	T/T	T/G	G/G			1.01 (0.83–1.23)
	none	none	Case	2,939 (0.92)	241 (0.08)	1,359 (0.85)	221 (0.14)	10 (0.01)	0.9750	0.9966	
	−8823		Control	2,298 (0.92)	190 (0.08)	1,062 (0.85)	174 (0.14)	8 (0.01)			

26	NKX6-1_SNP3			G	A	G/G	G/A	A/A			1.05 (0.95–1.17)
	rs1545330	JPT	Case	1,719 (0.54)	1,461 (0.46)	452 (0.28)	815 (0.51)	323 (0.20)	0.3348	0.5938	
	−8797		Control	1,312 (0.53)	1,176 (0.47)	338 (0.27)	636 (0.51)	270 (0.22)			
27	NKX6-1_SNP4			A	C	A/A	A/C	C/C			1.01 (0.90–1.13)
	rs2278671	JPT	Case	2,094 (0.66)	1,086 (0.34)	681 (0.43)	732 (0.46)	177 (0.11)	0.8884	0.5354	
	IVS2 + 28		Control	1,633 (0.66)	855 (0.34)	541 (0.43)	551 (0.44)	152 (0.12)			
28	NEUROD1_SNP1			C	G	C/C	C/G	G/G			1.03 (0.91–1.16)
	rs3916026	JPT	Case	893 (0.28)	2,287 (0.72)	132 (0.08)	629 (0.40)	829 (0.52)	0.6685	0.3769	
	−5425		Control	685 (0.28)	1,803 (0.72)	87 (0.07)	511 (0.41)	646 (0.52)			
29	NEUROD1_SNP2			G	T	G/G	G/T	T/T			1.03 (0.90–1.18)
	rs7420169	JPT	Case	2,538 (0.80)	642 (0.20)	1,022 (0.64)	494 (0.31)	74 (0.05)	0.6684	0.6459	
	−5084		Control	1,998 (0.80)	490 (0.20)	803 (0.65)	392 (0.32)	49 (0.04)			
30	ABCC8_SNP1			C	T	C/C	C/T	T/T			1.08 (0.97–1.20)
	rs1799854	JPT	Case	1,507 (0.47)	1,673 (0.53)	371 (0.23)	765 (0.48)	454 (0.29)	0.1664	0.0073†	
	IVS15 −3		Control	1,226 (0.49)	1,262 (0.51)	280 (0.23)	666 (0.54)	298 (0.24)			
31	ABCC8_SNP2			G	A	G/G	G/A	A/A			1.07 (0.91–1.25)
	rs4148643	JPT	Case	2,795 (0.88)	385 (0.12)	1,232 (0.77)	331 (0.21)	27 (0.02)	0.4419	0.7059	
	R1273R		Control	2,169 (0.87)	319 (0.13)	950 (0.76)	269 (0.22)	25 (0.02)			
32	ABCC8_SNP3			T	G	T/T	T/G	G/G			1.07 (0.96–1.19)
	rs757110	JPT	Case	1,884 (0.59)	1,296 (0.41)	570 (0.36)	744 (0.47)	276 (0.17)	0.2432	0.4293	
	S1369A		Control	1,513 (0.61)	975 (0.39)	463 (0.37)	587 (0.47)	194 (0.16)			
33	KCNJ11_SNP1			G	A	G/G	G/A	A/A			1.08 (0.97–1.21)
	rs5219	none	Case	1,954 (0.61)	1,226 (0.39)	610 (0.38)	734 (0.46)	246 (0.15)	0.1513	0.3343	
	E23K		Control	1,576 (0.63)	912 (0.37)	503 (0.40)	570 (0.46)	171 (0.14)			

Locus: experimental name of the SNP, followed by rs number and position. HapMap data: JPT, genotyped on Japanese in Tokyo. Nominal P values are listed for allele or genotype frequencies (*P <0.05; †P<0.01). IVS, intron variant sequence.